1969 SMITHSONIAN STANDARD EARTH AND GLOBAL TECTONICS

E. M. Gaposchkin, W. M. Kaula, and K. Lambeck

September 1970

009-49

1969 SMITHSONIAN STANDARD EARTH AND GLOBAL TECTONICS

E. M. Gaposchkin, W. M. Kaula, and K. Lambeck

ABSTRACT

Geodetic parameters describing the earth's gravity field and the positions of satellite-tracking stations in a geocentric reference frame have been computed. These parameters were estimated from a combination of four different types of data — routine and simultaneous satellite observations, observations of deep-space probes, and surface gravimetry.

The global gravity field is represented by spherical harmonics complete to degree and order 16, plus a number of coefficients to which satellites are sensitive, a resolution of about 11° or 1200 km.

The accuracy is established primarily by intercomparison. The coordinates of 12 fundamental stations are known to ±10 m or better, and those of 39 stations (or groups of collocated stations) are known to ±20 m or better. The accuracy of the global field is ±3 m in geoid height, or ±9 mgal.

This solution leads to a new understanding of global tectonics and geodynamics. It shows ocean rises, as well as trench and island arcs, as mass excesses. Ocean basins, areas of recent glaciation, and the Asian portion of the Alpide belt are mass deficiencies. Most features appear to be the result of varying behavior of the lithosphere in response to asthenospheric flow.

INTRODUCTION

An original objective of space science was the improvement of geodetic parameters "to tie together the observing stations and the center of the geoid to a precision of the order of 10 m, ... to add appreciably to knowledge of the density distribution in the earth, particularly in the crustal volumes"

009-49

(Whipple and Hynek, 1958). This objective has been achieved and surpassed, as demonstrated in 1966 with the publication by the Smithsonian Astrophysical Observatory (SAO) of numerical parameters for the earth's gravity field and the coordinates of satellite-tracking stations (Gaposchkin, 1967; Köhnlein, 1967a; Veis, 1967a, b; Whipple, 1967; Lundquist and Veis, 1966).

Four things were apparent in light of the 1966 results: 1) further work would be valuable, 2) both additional and other kinds of data could be profitably incorporated, 3) new observing techniques such as laser tracking would be important, and 4) other disciplines such as solid-earth geophysics and oceanography could be well served by what had previously been a wholly geodetic program.

These last two points were the focus of a series of seminars conducted at SAO (Lundquist and Friedman, 1966). A later and more comprehensive study along similar lines was conducted at Williamstown (Kaula, 1970). The latter part of this paper addresses itself to several aspects of earth physics in light of results from satellite geodesy.

The geodetic results in 1966 benefited from the use of two types of data — simultaneous observations and individual observations. The solution was strengthened by combining the data, and the accuracy was established by intercomparison rather than by reliance on formal statistics or internal consistency. Subsequently, other types of data were used; Köhnlein (1967b) made a combination of satellite and surface gravimetry, and Veis (1966) made a further comparison of station coordinates using Deep Space Net (DSN) data to determine the relative positions of the DSN antennas. The results in 1969 included these additional types of data as integral parts of the solution.

The geometry of Baker-Nunn stations in 1966 was poor in some regions. A series of station moves and subsequent observing programs produced a considerably improved geometrical determination, especially in South America. The data used in the dynamical solution were improved by a series of observations made specifically for this purpose, by an improvement in the reduction procedures, and by use of more accurate clocks at the stations.

A complete revision of the computer programs was initiated, with many of the theoretical aspects rediscussed.

Finally, the process of statistical inference was improved. Each type of data was treated consistently by establishing weights and covariances. Different sets of data were combined and relative weights were adopted, which improved the residuals for each set of data. For example, the terrestrial gravimetry was weighted so that the combined solution improved the orbits as well as reduced the RMS gravity-anomaly residuals. Once each type of data was internally consistent, reliability estimates could be established; and when each quantity had been determined by independent methods, a direct comparison of the estimates was possible. In this way, a realistic evaluation of the accuracy was possible.

In summary, a combination of four types of data gave the best estimate of geodetic parameters, and reliable estimates of the accuracy were provided by intercomparison. Further comparisons with data not used in the solution — orbital data, terrestrial gravimetry, astrogeodetic leveling, and triangulation — completely confirmed the accuracy obtained by intercomparison.

STRUCTURE OF THE PROCESS

The combination of four types of data is essentially an iterative process. The initial values for the gravity field and station coordinates were taken from the 1966 M1 solution, as modified by some resonant harmonics, and the C6 coordinates. The values of the zonal harmonics were revised by Kozai (1969) as a precursor to this analysis. In addition, three constants, defining the length and time scales — GM, a_e, and c — need to be chosen. Table 1 lists the coefficients and constants used throughout this analysis.

Figure 1 describes the information flow. Each component in Figure 1 is described in Gaposchkin and Lambeck (1970). The first two rows indicate very briefly the process before analysis. There are two major loops in the scheme. The large loop is a complete recalculation of the observation

3

TABLE 1.   Adopted zonal harmonics to J(21) (Kozai, 1969).

J(2) = 1.08262800E-03	J(3) = -2.5380E-06
J(4) = -1.5930E-06	J(5) = -2.3000E-07
J(6) = 5.0200E-07	J(7) = -3.6200E-07
J(8) = -1.1800E-07	J(9) = -1.0000E-07
J(10) = -3.5400E-07	J(11) = 2.0200E-07
J(12) = -4.2000E-08	J(13) = -1.2300E-07
J(14) = -7.3000E-08	J(15) = -1.7400E-07
J(16) = 1.8700E-07	J(17) = 8.5000E-08
J(18) = -2.3100E-07	J(19) = -2.1600E-07
J(20) = -5.0000E-09	J(21) = 1.4400E-07

$$GM = 3.986013 \times 10^{20} \ cm^3/sec^2$$

$$a_e = 6.378155 \times 10^6 \ m$$

$$c = 2.997925 \times 10^{10} \ cm/sec$$

SURFACE-
GRAVITY
MEASUREMENT

(Δg)

DEEP SPACE NET
OBSERVATION OF PROBES
5 STATIONS   JPL

$\dot{\rho}$

SATELLITE-TRACKING PROGRAM (SAO) AND
COOPERATING AGENCIES, WITH CAMERAS
AND ELECTRONIC TRACKING

SIMULTANEOUS EVENTS

SATURATION TRACKING

REDUCTION TO
5°×5° MEANS
(KAULA)

CALCULATION OF r, $\delta\lambda$
FOR
EACH STATION
ALSO Gm, $m_s/m_\oplus$ ETC.
(MOTTINGER)

GEOMETRICAL ADJUSTMENT
FOR DIRECTIONS BETWEEN
STATIONS
(ℓ,m,n)

ADOPT $C_{\ell m}$, $S_{\ell m}$, $\overline{X}_i$
SELECT UNKNOWNS
FOR DYNAMIC,
GEOMETRIC, AND
TOTAL SOLUTION

COMPUTE OBSERVATION
EQUATIONS FOR
$\Delta C_{\ell m}$

COMPUTE OBSERVATION
EQUATIONS FOR
Δr, $\Delta\delta\lambda$

COMPUTE
OBSERVATION EQUATION
FOR
$\Delta(\ell,m,n)$

COMPUTE ORBITAL ELEMENTS
FOR EACH ARC
THEN
COMPUTE OBSERVATION
EQUATIONS FOR
$\Delta C_{\ell m}$, $\overline{\Delta X}$

FORM
WEIGHTED NORMAL EQUATION

FORM
WEIGHTED NORMAL EQUATION

PERFORM ADJUSTMENT FOR
FOUR GROUPS OF STATIONS
SEPARATELY

FORM
WEIGHTED NORMAL EQUATION

COMBINE FOUR GROUPS VIA
COMMON STATIONS
FORMING NORMAL
EQUATIONS

SOLVE
WITH ASSUMPTION

SOLVE

SOLVE FOR
COORDINATES
BY FIXING
9010

SOLVE FOR
DIRECTIONS

SOLVE FOR
$\Delta C_{\ell m}$ AND
COORDINATES

SOLVE FOR
COORDINATES

COMBINE GEOMETRICAL
DATA

WEIGHT NORMALS AND
COMBINE

SOLVE

COMPARE
WITH SURFACE
GRAVIMETRY

COMPARE
DSN COORDINATES

COMPARE WITH
DIRECTION

COMPARE WITH
ORBITS
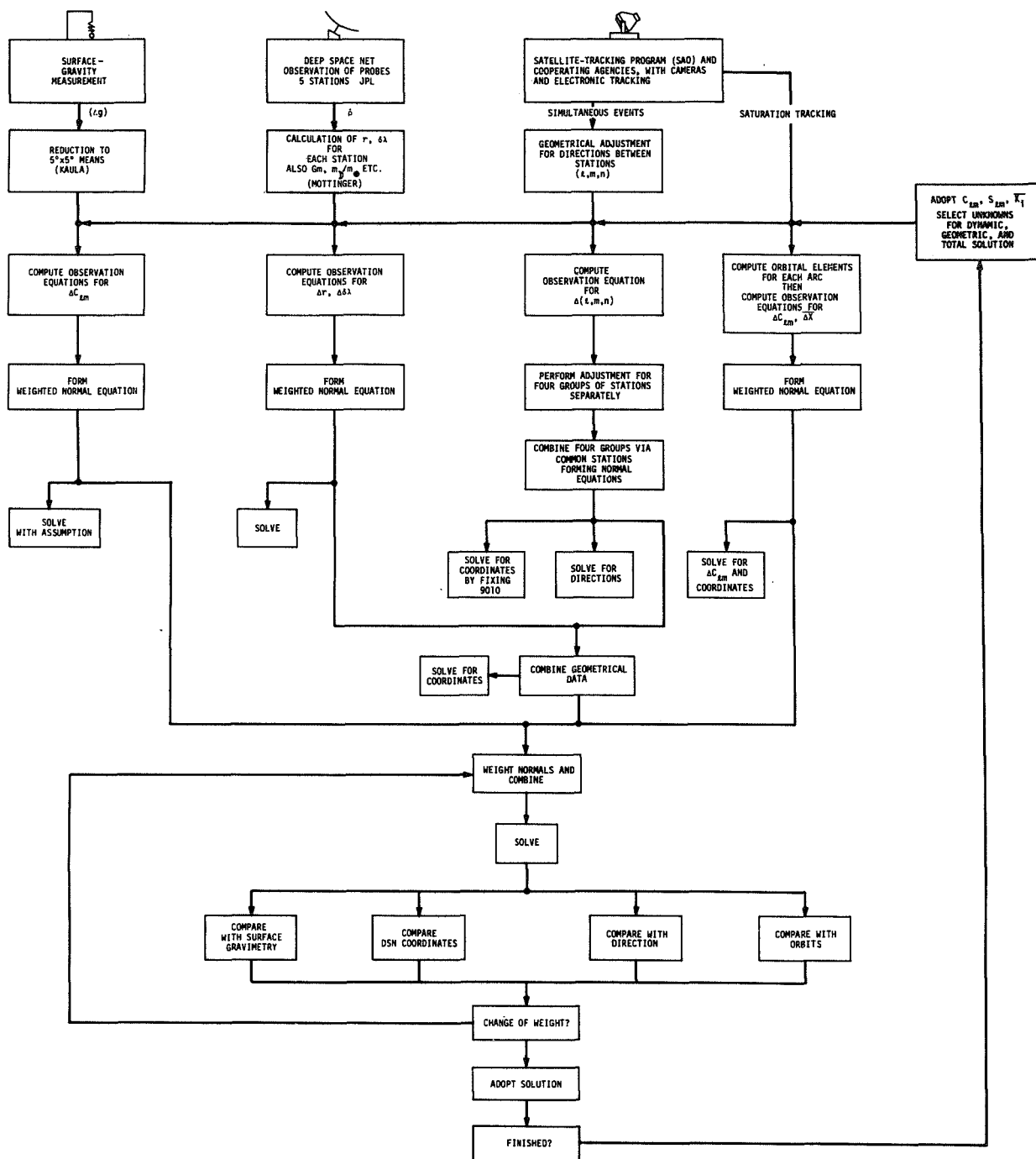
CHANGE OF WEIGHT?

ADOPT SOLUTION

FINISHED?

Fig. 1.   Structure of the process.

equations and residuals and could be called an iteration. Each separate set of data is solved independently, with some assumptions when necessary. These solutions and residuals are compared.

The second, smaller loop is used to determine the appropriate relative weights of the four components. The weights are chosen, a solution is calculated, and the residuals are investigated. If revision is necessary, the weights are changed and another solution is made. At this point, certain orbital information and geometric data may be either added or deleted if appropriate.

Each solution is compared with some independent orbits, as well as with the observations used in the solution and with the separate solutions themselves. In practice, five or six such solutions are calculated, and one is adopted for the subsequent analysis.

DATA USED

The position of the earth in the inertial reference frame is monitored, tabulated, and published in terms of pole position (x, y) and sidereal time (UT1) by the Bureau International de l'Heure (BIH), the United States Naval Observatory (USNO), and, for pole position only, the International Polar Motion Service (IPMS). The largest difference of the published values is 5 m in UT1, although it is impossible to tell what the correct values are and to establish further the real accuracy of these data. The position of the earth seems to be known to no better than several meters. The uncertainty in these data sets the limit of accuracy in station positions. For the analysis described here, we have adopted the UT1 data published by the BIH and the pole position published by the IPMS.

The locations of stations contributing satellite observations are indicated in Figure 2. There is a clustering of stations in North America and western Europe. Most of these stations contributed many simultaneous observations but of only a few satellites. These data were extremely valuable for a
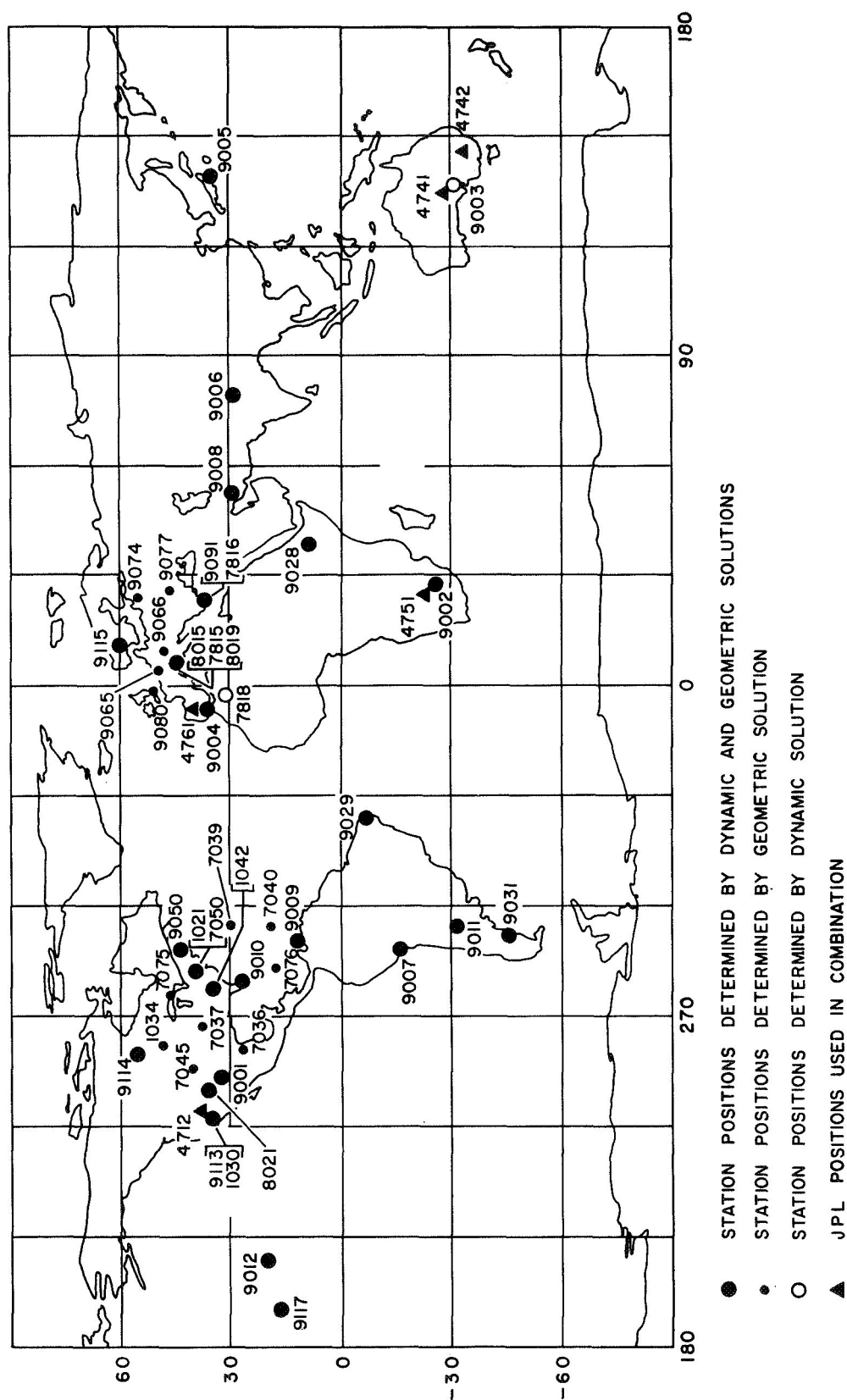
Fig. 2. Location of stations used in the combination solutions. Collocated stations are bracketed together.

STATION POSITIONS DETERMINED BY DYNAMIC AND GEOMETRIC SOLUTIONS

STATION POSITIONS DETERMINED BY GEOMETRIC SOLUTION

STATION POSITIONS DETERMINED BY DYNAMIC SOLUTION

JPL POSITIONS USED IN COMBINATION

geometrical net adjustment but were not appropriate for a dynamical determination of station coordinates. More than 50,000 observations were combined in the geometrical solution.

The final dynamical solution used more than 60,000 observed quantities on the 21 satellites listed in Table 2. The distribution of orbital characteristics is illustrated in Figure 3.

The DSN data from five stations were compiled by Mottinger (1969). Each DSN station can be related to a Baker-Nunn camera by the use of classical survey data. We then have for these stations additional observational constraints on the relative longitudes and the distance from the spin axis of the earth.

The terrestrial gravimetry data used in the solution were compiled by Kaula (1966) and consisted of 300-nautical-mile (n mi) free-air anomalies. His basic data consisted of $1° \times 1°$ mean free-air anomalies. The results were 935 mean anomalies for 300-n mi squares covering 56.5% of the globe.

Since the details of the analysis are given elsewhere, the following discussion is limited to the accuracy of the final results.

The final results for the geocentric cartesian station coordinates are given in Tables 3 and 4, and for the tesseral harmonics, in Table 5. Table 1 contains the precision estimates of the station coordinates, and Figure 4 gives the precision of the geoid height as a function of latitude. These estimates have been taken from the statistics of the final iteration, using the weighting factors from the combination, and are corroborated by all the intercomparisons. The geoid-height estimates, of course, refer to the generalized geoid only and do not imply that the geoid is known everywhere with this accuracy.

8

TABLE 2. Summary of dynamical data.

| Satellite	Name or Other Designation	Inclination (deg.)	Eccentricity	Semimajor Axis (km)	Perigee Height (km)	Number of Arcs	Days/Arc	New Satellite	Select Files	Laser Data
6001301	Courier 1B 60 ν1	28	0.016	7465	965	6	30	X	X	
5900101	Vanguard 2 59 α1	33	0.165	8300	557	7	30		X	
6100401	61 δ1	39	0.119	7960	700	3	14			X
6701401	D1D	39	0.053	7337	569	6	14	X	X	X
6701101	D1C	40	0.052	7336	579	4	14	X	X	X
6503201	Explorer 27 BE-C	41	0.026	7311	941	4	30	X	X	
6000902	60 ι2	47	0.011	7971	1512	7	30			
6206001	Anna 1B 62 βμ1	50	0.007	7508	1077	12	30		X	
6302601	Geophysical Research	50	0.062	7237	424	6	14			
6508901	Explorer 29 Geos 1	59	0.073	8074	1121	21	30	X	X	X
6101501	Transit 4A 61 o1	67	0.008	7318	885	8	30			
6101502	Injun 1 61 o2	67	0.008	7316	896	4	30			
6506301	Secor 5	69	0.079	8159	1137	2	30	X	X	
6400101		70	0.002	7301	921	3	30	X		
6406401	Explorer 22 BE-B	80	0.012	7362	912	2	30	X		X
6508101	OGO 2	87	0.075	7344	420	2	14	X		
6600501	Oscar 07	89	0.023	7417	868	1	30	X	X	
6304902	5BN-2	90	0.005	7473	1070	5	30	X		
6102801	Midas 4 61 αδ1	96	0.013	10005	3503	3	50			
6800201	Explorer 36 Geos 2	106	0.031	7709	1101	6	14	X		X
6507801	OV1 2	144	0.182	8306	416	2	14	X		
						114				

9
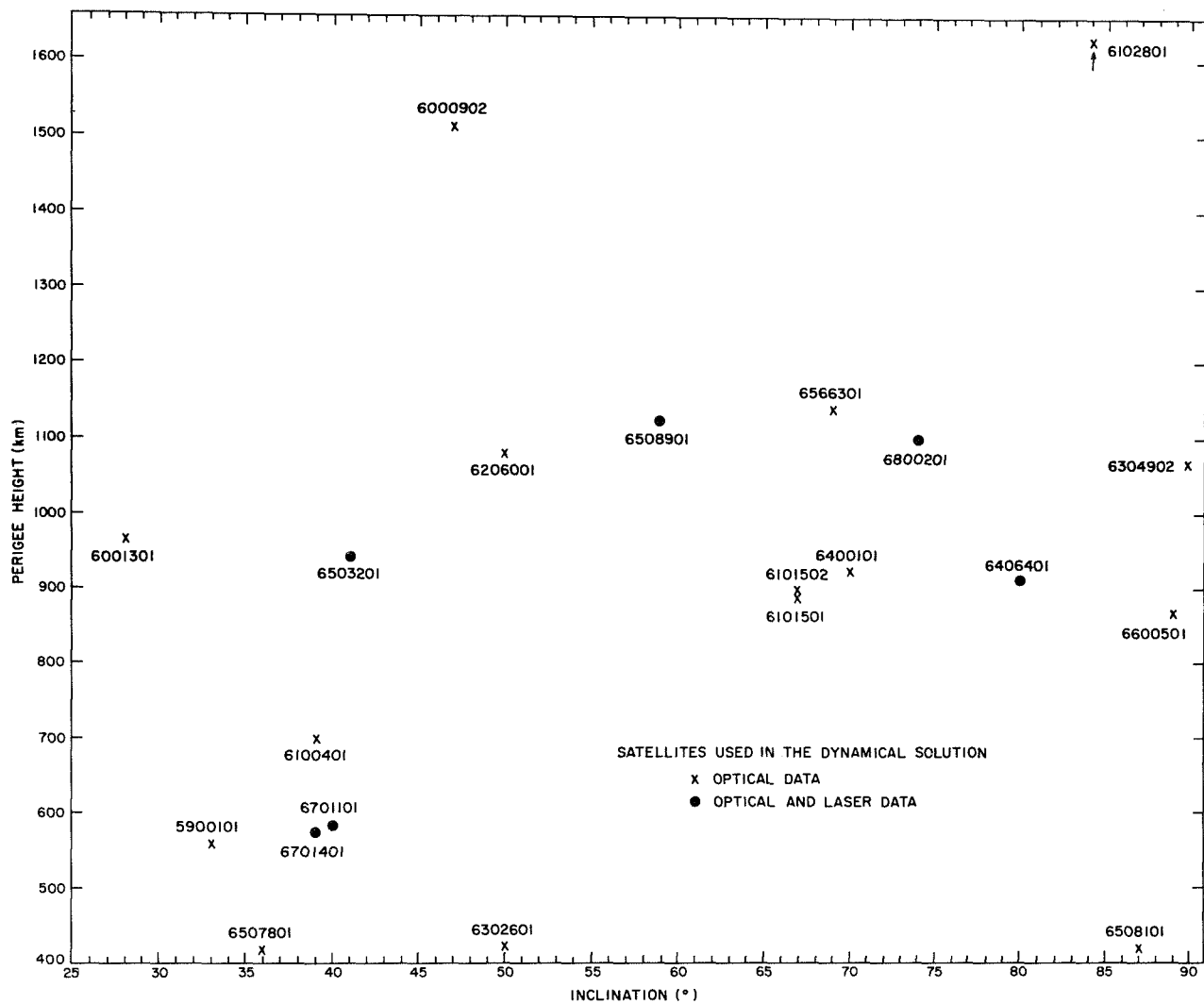
Fig. 3. Distribution of satellites used in the 1969 Smithsonian Standard Earth (II) (Gaposchkin and Lambeck, 1970).

TABLE 3. Geocentric coordinates (in Mm) of the stations determined in the final combination solution. The fifth column gives the formal precision estimates of the coordinates in meters.

Station	X	Y	Z	σ	Station Name
1021	1.118029	-4.876316	3.942984	7	BLOSSOM POINT, MD.
1034	-.521702	-4.242049	4.718731	7	GRAND FORKS, MINN.
1042	.647515	-5.177924	3.656707	7	ROSMAN, N. C.
7036	-.828496	-5.657458	2.816812	7	EDINBURG, TEX.
7037	-.191286	-4.967280	3.983262	7	COLUMBIA, MO.
7039	2.308239	-4.873597	3.394580	10	BERMUDA
7040	2.465067	-5.534924	1.985510	10	PUERTO RICO
7045	-1.240479	-4.760229	4.048995	9	DENVER, COL.
7050	1.130674	-4.831368	3.994111	7	Goddard Space Flight Center
7075	.692628	-4.347059	4.600483	9	SUDBURY, ONT.
7076	1.384174	-5.905685	1.966533	10	JAMAICA
7815	4.578370	.457951	4.403134	5	HAUTE PROVENCE, FRANCE
7816	4.654337	1.959134	3.884366	5	STEPHANION, GREECE
7818	5.426329	-.229330	3.334608	15	COLOMB-BECHAR, ALGERIA
7901	-1.535757	-5.166996	3.401042	5	ORGAN PASS, N.M.
8015	4.578328	.457966	4.403179	5	HAUTE PROVENCE, FRANCE
8019	4.579466	.586599	4.386408	5	NICE, FRANCE
9001	-1.535757	-5.166996	3.401042	5	ORGAN PASS, N.M.
9002	5.056125	2.716511	-2.775784	7	PRETORIA, S.AFRICA
9003	-3.983776	3.743087	-3.275566	6	WOOMERA, AUSTRALIA
9004	5.105588	-.555228	3.769667	5	SAN FERNANDO, SPAIN
9005	-3.946693	3.366299	3.698832	10	TOKYO, JAPAN
9006	1.018203	5.471103	3.109623	9	NAINI TAL, INDIA
9007	1.942775	-5.804081	-1.796933	7	AREQUIPA, PERU
9008	3.376893	4.403976	3.136250	9	SHIRAZ, IRAN
9009	2.251829	-5.816919	1.327160	7	CURACAO, ANTILLES
9010	.976291	-5.601398	2.880240	5	JUPITER, FLA.
9011	2.280589	-4.914573	-3.355426	9	VILLA DOLORES, ARGENTINA
9012	-5.466053	-2.404282	2.242171	7	MAUI, HAWAII
9021	-1.936782	-5.077704	3.331916	15	MT. HOPKINS, ARIZ.
9023	-3.977766	3.725102	-3.303035	6	ISLAND LAGOON, AUSTRALIA
9025	-3.910437	3.376361	3.729217	10	DODAIRA, JAPAN
9028	4.903750	3.965201	.963872	12	ADDIS ABABA, ETHIOPIA
9029	5.186461	-3.653856	-.654325	12	NATAL, BRAZIL
9031	1.693803	-4.112328	-4.556649	15	COMODORO RIVADAVIA, ARGENTINA
9050	1.489753	-4.467478	4.287304	14	HARVARD, MASS.
9065	3.923411	.299882	5.002945	12	DELFT, HOLLAND
9066	4.331310	.567511	4.633093	7	ZIMMERWALD, SWITZERLAND
9074	3.183901	1.421448	5.322772	10	RIGA, LATVIA
9077	3.907421	1.602397	4.763890	10	UZGHOROD, U.S.S.R.
9080	3.920178	-.134738	5.012708	9	MALVERN, ENGLAND
9091	4.595157	2.039425	3.912650	5	DIOYSOS, GREECE
9113	-2.450011	-4.624421	3.635035	7	ROSAMUND, CAL.
9114	-1.264838	-3.466884	5.185467	12	COLD LAKE, CANADA
9115	3.121280	.592643	5.512701	17	Harestua, Norway
9117	-6.007402	-1.111859	1.825730	15	JOHNSTON ISL., PACIFIC

TABLE 4. Coordinates of the JPL stations referred to the SAO
reference system.

Station	X (Mm)	Y (Mm)	Z (Mm)
4751	5.085451	2.668252	-2.768728
4741	-3.978706	3.724858	-3.302213
4742	-4.460972	2.682424	-3.674618
4761	4.849242	-0.360290	4.114869
4712	-2.350454	-4.651975	3.665631
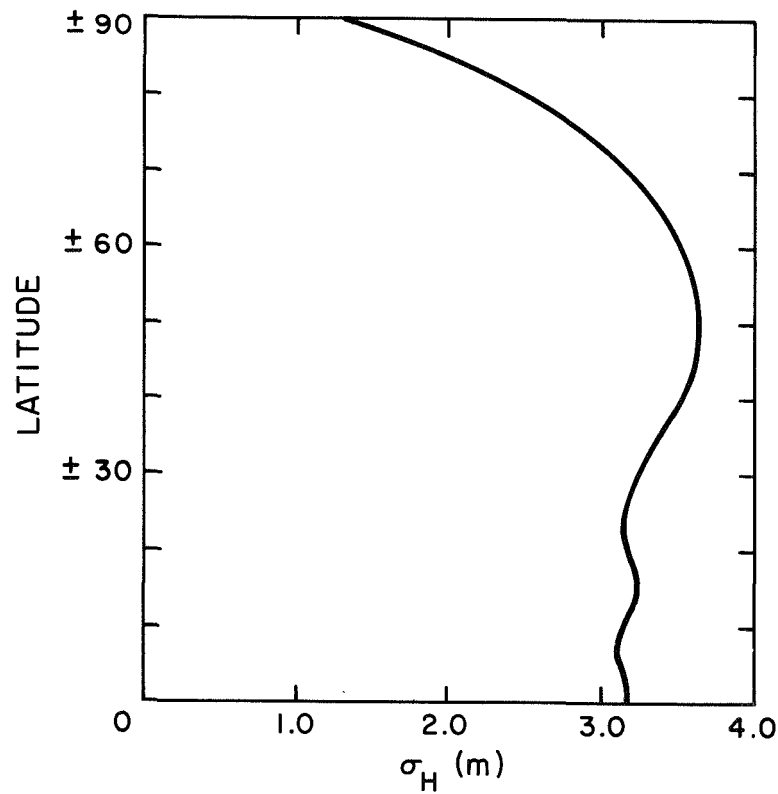
Fig. 4. Precision estimates of geoid heights determined from the harmonic
coefficient precision estimates.

TABLE 5. Fully normalized coefficients of the spherical harmonic expansion of the geopotential obtained in the final iteration of the combination solution. $C_{\ell m}$ are the cosine terms of degree ℓ and order m and $S_{\ell m}$ are the sine terms.

ℓ	m	$C_{\ell m}$	$S_{\ell m}$	ℓ	m	$C_{\ell m}$	$S_{\ell m}$
2	2	2.4129E-06	-1.3641E-06	3	1	1.9698E-06	2.6015E-07
3	2	8.9204E-07	-6.3468E-07	3	3	6.8630E-07	1.4304E-06
4	1	-5.2989E-07	-4.8765E-07	4	2	3.3024E-07	7.0633E-07
4	3	9.8943E-07	-1.5467E-07	4	4	-7.9692E-07	3.3928E-07
5	1	-5.3816E-08	-9.7905E-08	5	2	6.1286E-07	-3.5087E-07
5	3	-4.3083E-07	-8.6663E-08	5	4	-2.6693E-07	8.3010E-08
5	5	1.2593E-07	-5.9910E-07	6	1	-9.8984E-08	3.7652E-08
6	2	5.4825E-08	-3.5175E-07	6	3	2.7873E-08	4.4626E-08
6	4	-4.0342E-10	-4.0388E-07	6	5	-2.1143E-07	-5.2264E-07
6	6	8.8693E-08	-7.4756E-08	7	1	2.4142E-07	1.1567E-07
7	2	2.8306E-07	1.5645E-07	7	3	2.0285E-07	-2.3448E-07
7	4	-1.9727E-07	-1.1390E-07	7	5	-8.7024E-10	9.8461E-08
7	6	-2.5847E-07	1.0209E-07	7	7	1.5916E-07	-6.7710E-08
8	1	3.1254E-08	2.5696E-08	8	2	4.8161E-08	8.4140E-08
8	3	-5.7444E-08	1.8086E-08	8	4	-1.5378E-07	7.5264E-08
8	5	-5.6733E-08	6.1636E-08	8	6	-5.3903E-08	2.5930E-07
8	7	3.4390E-08	8.9168E-08	8	8	-7.7364E-08	6.7607E-08
9	1	1.3823E-07	-1.6100E-08	9	2	6.6741E-09	-8.1733E-08
9	3	-9.6463E-08	-1.1817E-07	9	4	5.7125E-08	1.1183E-07
9	5	-6.1435E-09	3.3551E-09	9	6	2.4186E-08	2.2028E-07
9	7	-5.0450E-08	-1.2700E-07	9	8	2.3359E-07	5.7239E-08
9	9	-8.2490E-08	9.2326E-08	10	1	1.1251E-07	-1.0167E-07
10	2	-3.1225E-08	-1.0450E-07	10	3	-2.3346E-08	-1.4137E-07
10	4	-4.8185E-08	-4.3248E-08	10	5	-8.0004E-08	-1.4279E-07
10	6	-3.2486E-08	-2.0153E-07	10	7	5.4961E-08	3.2003E-08
10	8	7.3957E-08	-7.9706E-08	10	9	-6.8563E-08	6.2498E-09
10	10	1.2377E-07	-2.5885E-08	11	1	4.3900E-09	2.9751E-08
11	2	4.8900E-08	-9.1994E-08	11	3	-6.3247E-08	-1.3109E-07
11	4	-3.0193E-08	5.4317E-08	11	5	3.2523E-08	1.3215E-07
11	6	3.7517E-08	6.9005E-09	11	7	4.5726E-08	-1.3862E-07
11	8	6.4546E-08	-1.6993E-08	11	9	1.1750E-07	-9.9451E-09
11	10	-1.1736E-07	-1.8900E-08	11	11	1.1785E-07	-4.0688E-08
12	1	-4.5955E-08	-3.1000E-08	12	2	2.7481E-08	7.5986E-08
12	3	5.8386E-08	5.4784E-08	12	4	-4.3649E-08	-2.2262E-08
12	5	2.3375E-08	4.2637E-08	12	6	-2.3868E-08	-6.6770E-10
12	7	1.4507E-08	9.9784E-08	12	8	-5.7854E-09	3.3752E-08
12	9	-3.2232E-08	4.2858E-08	12	10	-1.8590E-08	4.8382E-09
12	11	-4.4921E-08	-4.8206E-08	12	12	-1.9407E-08	-5.7771E-08
13	1	-5.6042E-08	2.6288E-08	13	2	-4.7456E-08	1.7367E-08
13	3	2.3833E-08	-2.8930E-08	13	4	-1.9980E-08	5.7030E-08
13	5	9.6637E-08	-4.7760E-08	13	6	-8.3417E-08	5.9782E-08
13	7	-5.2217E-08	-3.2562E-08	13	8	-4.1759E-08	-2.0231E-08
13	9	-2.5623E-08	1.0767E-07	13	10	8.6589E-08	-1.0528E-08
13	11	-3.3749E-08	5.8541E-08	13	12	-1.3229E-09	8.2192E-08
13	13	-7.0288E-08	7.4643E-08	14	1	-2.3090E-08	4.9664E-08
14	2	3.2120E-08	-4.5289E-08	14	3	1.9042E-08	1.1919E-09
14	4	7.8017E-09	-3.7527E-08	14	5	-2.5958E-08	-2.3344E-08
14	6	1.9140E-08	-5.8721E-08	14	7	1.1061E-08	8.4132E-09
14	8	-3.0273E-08	-6.0838E-08	14	9	4.9539E-08	9.2345E-08
14	10	5.3732E-08	-4.3168E-08	14	11	2.7833E-08	-8.1637E-08
14	12	1.2481E-08	-5.7314E-08	14	13	5.1554E-08	4.5453E-08
14	14	-5.2082E-08	-1.2840E-08	15	1	-3.5971E-09	4.0142E-08
15	2	-4.4833E-08	-1.6056E-08	15	3	8.3016E-09	-5.7218E-09
15	4	1.3916E-08	6.6644E-08	15	5	3.1684E-08	1.8250E-09
15	6	7.0020E-08	-1.1872E-07	15	7	1.1856E-07	4.2690E-08
15	8	-9.7657E-08	-3.5710E-08	15	9	2.2064E-08	2.6632E-08
15	10	-2.0648E-08	5.3724E-10	15	11	-3.2585E-08	9.4052E-08
15	12	1.0524E-08	6.8726E-09	15	13	-3.7348E-08	4.0249E-09
15	14	1.2193E-08	-2.6786E-08	15	15	1.4515E-09	-1.4802E-08
16	1	-2.3789E-08	7.6413E-08	16	2	2.1327E-08	3.0669E-08
16	3	-4.7358E-08	3.2610E-08	16	4	-1.1591E-08	4.3001E-08
16	5	-4.4201E-08	3.2230E-08	16	6	-5.8439E-08	-4.2809E-08
16	7	1.0591E-07	8.1008E-09	16	8	-8.4738E-08	-2.4677E-09
16	9	9.0001E-09	-1.0628E-07	16	10	-2.9849E-08	-5.2467E-10
16	11	6.8502E-09	-7.0765E-08	16	12	2.2834E-08	-3.4087E-08
16	13	3.5475E-08	2.0683E-08	16	14	-7.3590E-09	-2.2626E-08
16	15	-3.5485E-08	8.4126E-10	16	16	-2.9522E-08	8.6217E-09
17	12	8.3097E-08	3.5424E-09	17	13	3.2749E-08	4.2920E-10
17	14	-1.6058E-08	2.7286E-08	18	12	1.1662E-08	8.4724E-09
18	13	4.6903E-08	-3.5547E-08	18	14	-2.7446E-08	-4.8376E-08
19	12	6.7115E-08	-8.2623E-09	19	13	3.3201E-08	-6.3128E-08
19	14	-3.9779E-09	-2.3817E-08	20	13	5.8374E-08	3.3320E-08
20	14	1.1130E-08	-1.6183E-08	21	13	3.6928E-09	-1.6288E-08
21	14	5.2067E-08	3.0801E-10	22	14	-8.0549E-09	2.6440E-08

13

COMPARISON WITH SATELLITE ORBITS

Each iteration resulted in improved orbital residuals using the combination solution. For the final solution, the orbital residuals for satellites such as Geos 1 and Geos 2 are less than 10 m. These 30-day orbits are computed from a combination of laser and Baker-Nunn data. The optical-data residuals have an RMS less than 3 arcsec, and the laser data residuals have an RMS value of 7 m. These residuals are, of course, made up of observation errors, model errors, errors in station coordinates, and errors in the gravity field.

COMPARISON OF GEOMETRIC AND DYNAMIC SATELLITE SOLUTIONS

Figure 5 compares directions between stations resulting from the geometric solution ($\triangle$), the dynamic solution ($\square$), and the combination solution ($\diamondsuit$). The difference in the positions derived from the individual solutions is a good indication of their relative accuracies and of the accuracy of the combination solution. These differences result from uncertainties in the coordinates at both stations, and at each station a number of such comparisons can usually be made. The comparisons shown here are the most unfavorable in that the errors of both stations are reflected in the comparison. Thus, the accuracy of the station positions of the combination solution, relative to the earth's center of mass, should be somewhat better than these figures indicate.

These comparisons indicate that for the fundamental Baker-Nunn stations (those numbered 9001 to 9012 and 9023) the combination-solution coordinates should be reliable to better than 10 m. For the new Baker-Nunn stations (9021, 9028, 9029, 9031, and 9091), from which there are fewer observations, the combination-solution coordinates should be accurate to better than 15 m. These estimates are in agreement with the formal statistics given in Table 3. The longitude difference between the two satellite solutions obtained from the combination solution is -0.2 ± 0.5 μrad and is not significant.

14
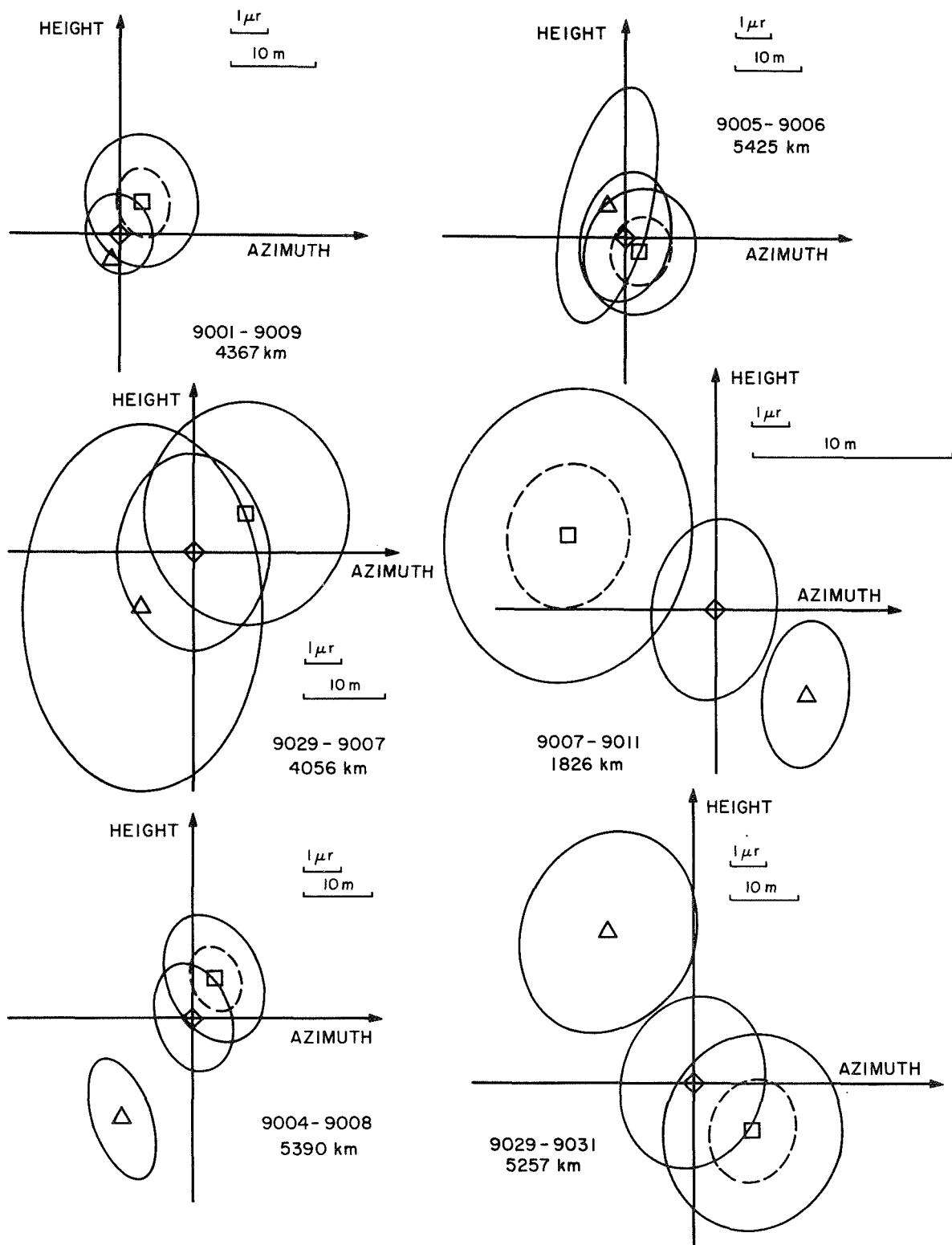
Fig. 5. Comparisons for station-station vectors computed from the geometric solution △, the dynamic solution □, and the combination solution ◇. The two error ellipses centered at □ refer to the formal statistics of the dynamic solution (the inner ellipse) and after the covariance matrix has been multiplied by the factor k_1^2 (outer ellipse).

15

COMPARISON OF SATELLITE AND DSN SOLUTIONS

The DSN sites can be related to Baker-Nunn station positions by ground survey. For three station groups (9002-4751), (9003-4741), and (9113-4712), the distance between the two instrumentation types does not exceed 200 km. For the other two groups (9003-4742) and (9004-4761), the distances are larger, about 500 and 1000 km, respectively, and uncertainties in the ground-survey information may influence the comparison results. Table 6 gives the results in the form of differences in longitude $\Delta\lambda_i$ and in distance to the earth's instantaneous rotation axis Δr_i. The table also gives the accuracy estimates deduced from the statistics of the two solutions and the ground-survey data. The comparisons reflect a systematic longitude difference, $\overline{\Delta\lambda} = -3.2$ μrad (the DSN longitudes are east of the SAO longitudes). When this systematic part is removed, the residuals are all less than about 10 m and support the accuracy estimates given in Table 3 for the Baker-Nunn stations 9002, 9003, 9004, and 9113.

COMPARISON WITH TERRESTRIAL GRAVIMETRY

Table 7 summarizes the comparison of the geopotential derived from (1) the new combination solution presented here, (2) the new satellite solution, and (3) the 1966 Standard Earth solution (also known as the M1 solution), using 300-n mi squares, for which at least 20 surveyed 60-n mi squares were available for the compilation. The comparisons are made for the three fields truncated at different degrees as well as for the total fields.

The quantities in Table 7 have been defined by Kaula (1966) and Gaposchkin and Lambeck (1970). Briefly, g_T is the terrestrial gravity anomaly and g_S is the satellite or combination solution anomaly; ϵ_T and ϵ_S are the expected errors in the estimates g_T and g_S, and δg is the expected truncation error. The estimate D of the gravity field contained by the spherical-harmonic expansion is obtained from the surface gravity. If both the satellite solution and the surface gravity give "perfect" results for all terms up to a certain degree, then

TABLE 6. Results of SAO-JPL stations comparison. $\Delta\lambda_i$ is the longitude difference and Δr_i the difference in distance to the earth's axis of rotation for the two solutions. $\overline{\Delta\lambda}$ is the weight mean longitude difference.

Stations	$\lambda_{SAO} - \lambda_{JPL} = \Delta\lambda_i$ (μrad)	$\overline{\Delta\lambda} - \Delta\lambda_i$ (μrad)	(m)	$\sigma_{\Delta\lambda_i}$ (m)	$r_{SAO} - r_{JPL} = \Delta r_i$ (m)	$\sigma_{\Delta r_i}$ (m)
4751-9002	-3.5	+0.3	+1.9	7.7	+5.9	4.9
4741-9003	-2.2	-0.9	-5.2	6.8	-7.3	4.5
4742-9003	-1.2	-2.0	-10.4	9.0	-6.5	4.5
4761-9004	-4.5	+1.4	+6.9	6.6	-1.2	4.5
4712-9113	-4.9	+1.7	+9.2	12.4	+7.6	5.5

TABLE 7. Comparison of satellite and combination solutions with surface-gravity measurements ($mgal^2$).

Solution	$\langle (g_T-g_S)^2 \rangle$	$\langle g_T g_S \rangle$	$\langle g_S^2 \rangle$	D	$\langle g_T^2 \rangle$	$E\{\epsilon_S^2\}$	$E\{\epsilon_T^2\}$	$E\{\delta g^2\}$
			$n \geq 20$,	$N = 136$,	300-n mi squares			
Combination Solution								
$\ell \leq 8$ $m \leq 8$	165	90	92	102	253	2	11	152
$\ell \leq 10$ $m \leq 10$	132	119	116	120	253	-3	11	123
$\ell \leq 11$ $m \leq 11$	135	126	134	126	253	8	11	116
$\ell \leq 12$ $m \leq 12$	134	129	138	129	253	9	11	113
$\ell \leq 14$ $m \leq 14$	109	156	166	146	253	10	11	87
$\ell \leq 16$ $m \leq 16$	75	184	186	163	253	2	11	58
			$n \geq 20$,	$N = 136$,	300-n mi squares			
Satellite Solution								
$\ell \leq 8$ $m \leq 8$	179	86	98	102	253	12	11	156
$\ell \leq 10$ $m \leq 10$	145	109	110	120	253	1	11	133
$\ell \leq 11$ $m \leq 11$	151	115	126	126	253	11	11	127
$\ell \leq 12$ $m \leq 12$	163	111	128	129	253	17	11	131
$\ell \leq 14$ $m \leq 14$	173	117	150	146	253	33	11	125
Total Field	177	118	161	143	253	43	11	124
			$n \geq 20$,	$N = 136$,	300-n mi squares			
M1 Solution								
$\ell \leq 8$ $m \leq 8$	168	85	85	102	253	0	11	157
Total Field	168	93	101	108	253	7	11	148

18

$$\langle g_S^2 \rangle = \langle g_T g_S \rangle = D$$

and

$$E\{\epsilon_S^2\} = E\{\epsilon_T^2\} = 0 \quad .$$

The combination solution gives the best results, in that there is good agreement between the three estimates $\langle g_S^2 \rangle$, $\langle g_T g_S \rangle$, and D of the true value of the contribution to the gravity anomaly from the geopotential coefficients. Also, the $E\{\epsilon_T^2\}$ and $E\{\epsilon_S^2\}$ are small. This might have been expected, since the combination solution contains the data against which the tests were made.

The estimates of the errors of omission $E\{\delta g^2\}$ are still quite large compared to the estimates of ϵ_S^2 and ϵ_T^2, a fact that indicates that the surface-gravity data contain some additional information that has not been extracted in this solution.

There is no significant difference between the satellite solution, the combination solution, and the M1 solution truncated to 8,8. Beyond degree 10, the combination is superior and the high-degree terms are determined primarily by the surface-gravity data.

Further comparisons with surface gravimetry are possible. There are compilations by Talwani and Le Pichon (1969) for the Atlantic Ocean and by Le Pichon and Talwani (1969) for the Indian Ocean. Figure 6 shows free-air gravity-anomaly profiles computed from 5° × 5° area means obtained from these compilations and from the combination solution. All profiles are referenced to the international gravity formula. The accuracy of the 5° × 5° area means is assumed to be 5 mgals. Table 8 gives $\langle (g_S - g_T)^2 \rangle$ for each of these profiles, and from these numbers the accuracy of the gravity anomalies computed from the combination solution can be determined. The average value is 10 mgal, or about 3.5 m in geoid height, in very good agreement with the value $\sqrt{75}$ mgal taken from Table 7.

19
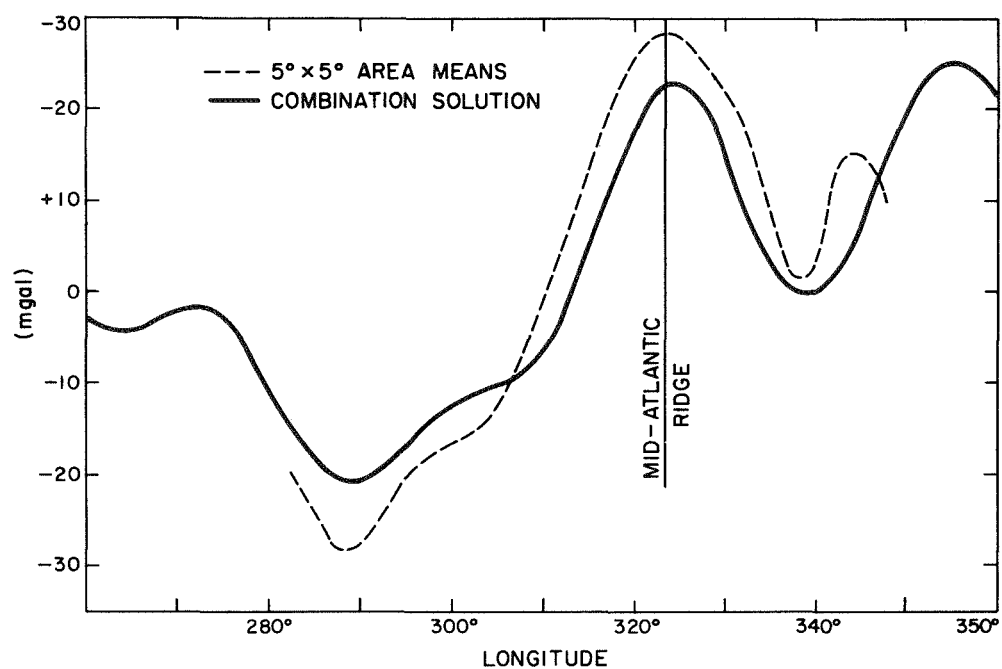
North Atlantic
$\Phi = +32°5$
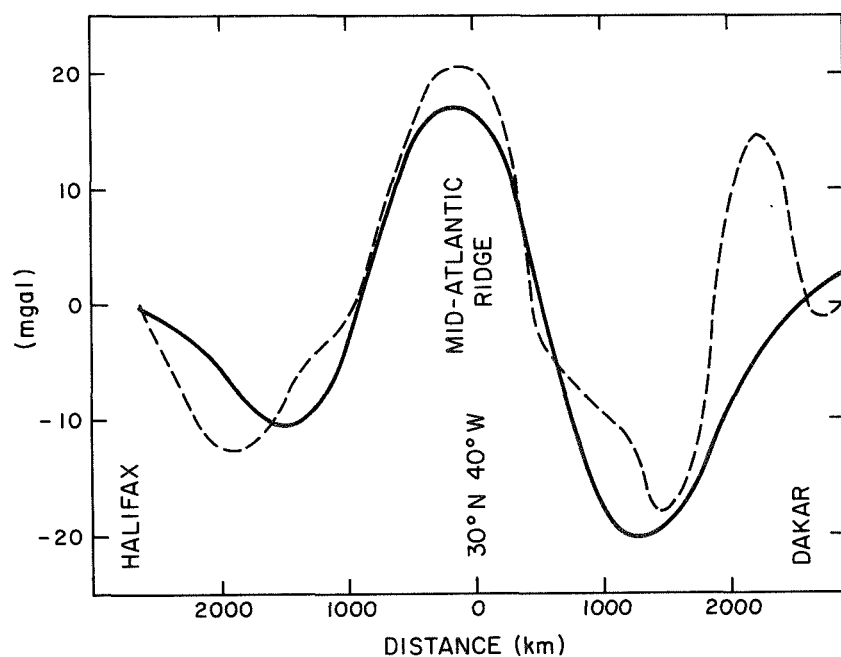
North Atlantic
Northwest—Southeast
Profile from Halifax to Dakar

Fig. 6. Comparisons of continuous gravity profiles from shipboard measurements compiled by Talwani and Le Pichon (broken lines) with profiles computed from the combination solution (solid lines).

20
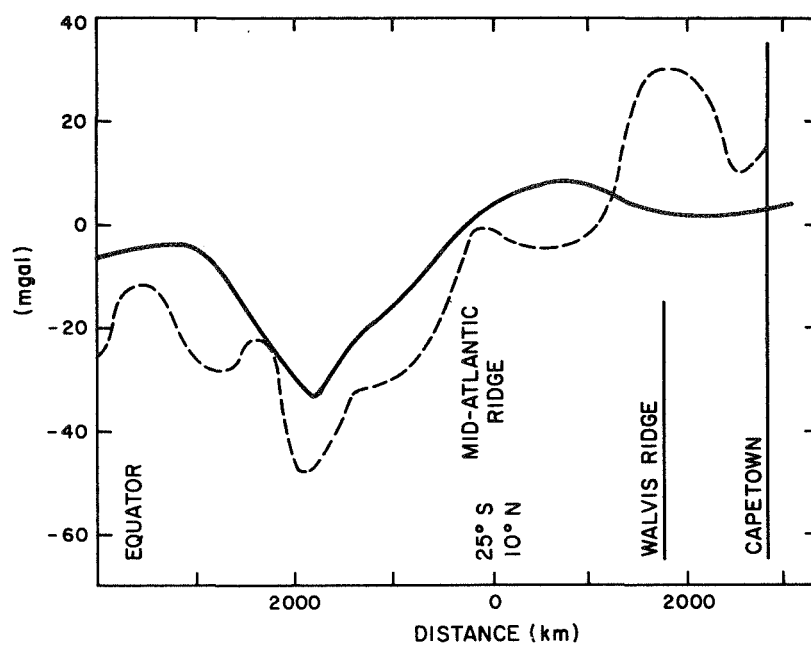
South Atlantic
Northwest—Southeast
Profile from Equator to Capetown
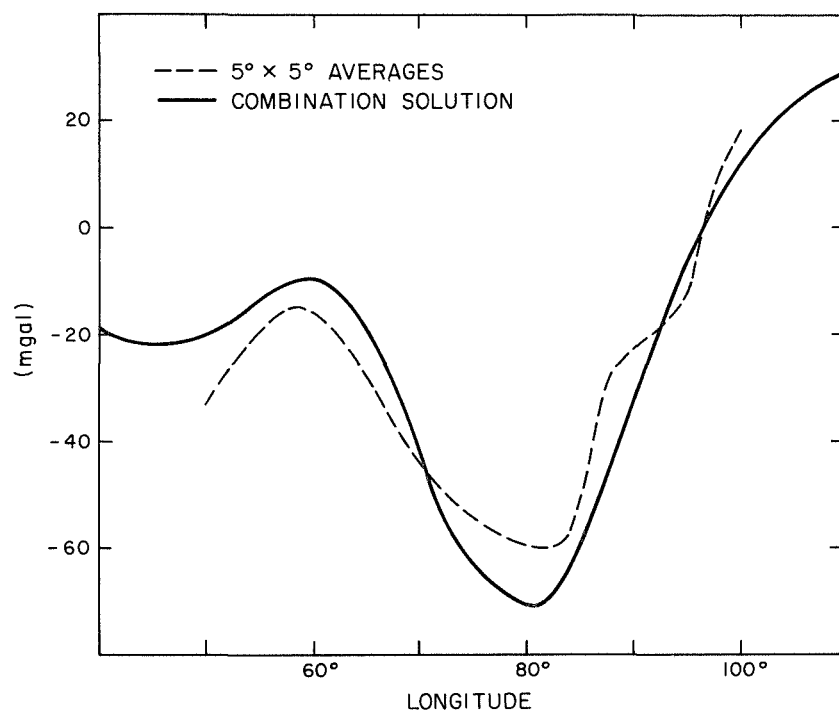
Indian Ocean
$\Phi = 0°$

Fig. 6 (Cont.)
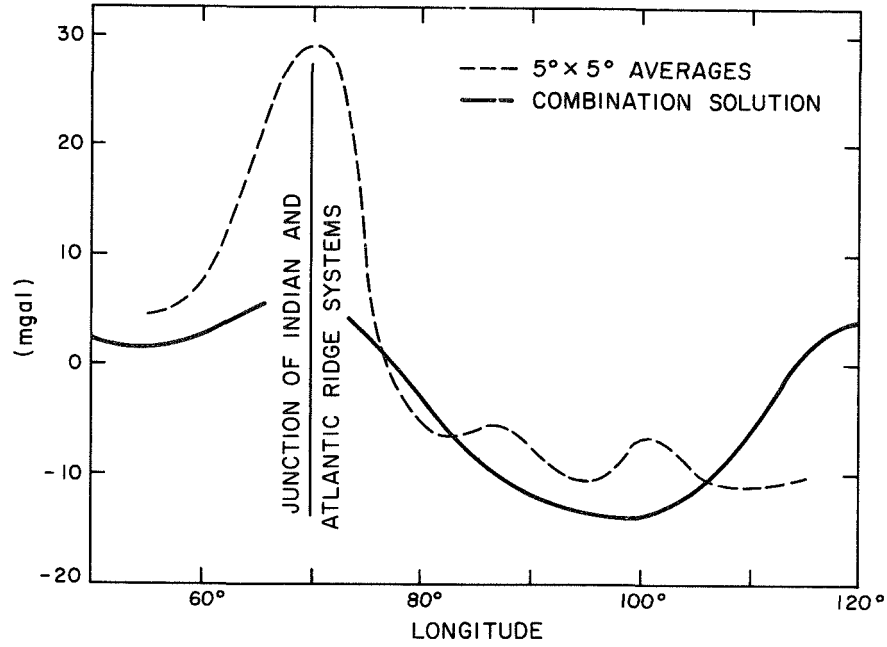
Indian Ocean
$\Phi = -25°$

Fig. 6 (Cont.)

TABLE 8. Summary of comparisons between surface-gravity measurements g_T by Talwani and Le Pichon and gravity anomalies g_S computed from the combination solution for selected profiles.

Profile	$\langle (g_S - g_T)^2 \rangle$ (mgal^2)	$\sigma^2_{g_T}$ (mgal^2)	$\sigma^2_{g_S} = \langle (g_S - g_T)^2 \rangle - \sigma^2_{g_T}$ (mgal^2)
$\phi = 32°5$ North Atlantic	84	25	59
NW-SE North Atlantic	68	25	43
NW-SE South Atlantic	222	25	197
$\phi = 0°$ Indian Ocean	80	25	55
$\phi = -25°$ Indian Ocean	166	25	144

$$(\sigma^2_{g_S})_{AV} = 99 \text{ mgal}^2 \approx 10 \text{ m}^2$$

22

COMPARISON WITH ASTROGEODETIC DATA

Geoid heights obtained from astrogeodetic leveling are available for several major datums. These data, like the surface-gravity data, could be used as further input to the combination solution. However, the coverage extends only to areas where reliable surface-gravity data are also available, and the contribution to the global solution would be limited. Instead, the astrogeodetic data have been used for comparison purposes, thus providing an independent estimate of the accuracy of the global solution.

For comparison, these geoids must be transformed to a geocentric reference system. Such a transformation can be established through a comparison of geodetic datum coordinates with coordinates derived from satellite analyses (Lambeck, 1970).

Figure 7 gives the geoids and the difference once the adjustment has been made. Table 9 gives the numerical differences; the $\sqrt{10.5}$ m is in excellent agreement with other accuracy estimates.

POWER SPECTRA

Table 10 gives the degree variances of the solution. As usual, the gravimetric solution gives underestimates of the degree variances. Figure 8 plots the same information, in addition to the $10^{-5}/\ell^2$ law, which fits the data very well. The standard deviation for each degree is also plotted. It is apparent that between degrees 18 and 20 the amplitude of the harmonic coefficients will be smaller than their uncertainties. The same limit is seen by an examination of $E\{\delta g^2\}$ from Table 7. We can estimate that the remaining 58 mgal^2 of information is completely contained in degrees 17 through 20. This is to some extent surprising, since we would expect that as 20th-degree terms have a half-wavelength of 9°, 5° $\times$ 5° anomalies would contain information of greater detail. Surface gravimetry certainly has a great deal of high-frequency detail. The methods for reducing the data to 1° $\times$ 1° squares and then to 5° $\times$ 5° squares may smooth the higher frequency data, or it

$\phi = 35°$

$\lambda = 260°$

North American Datum
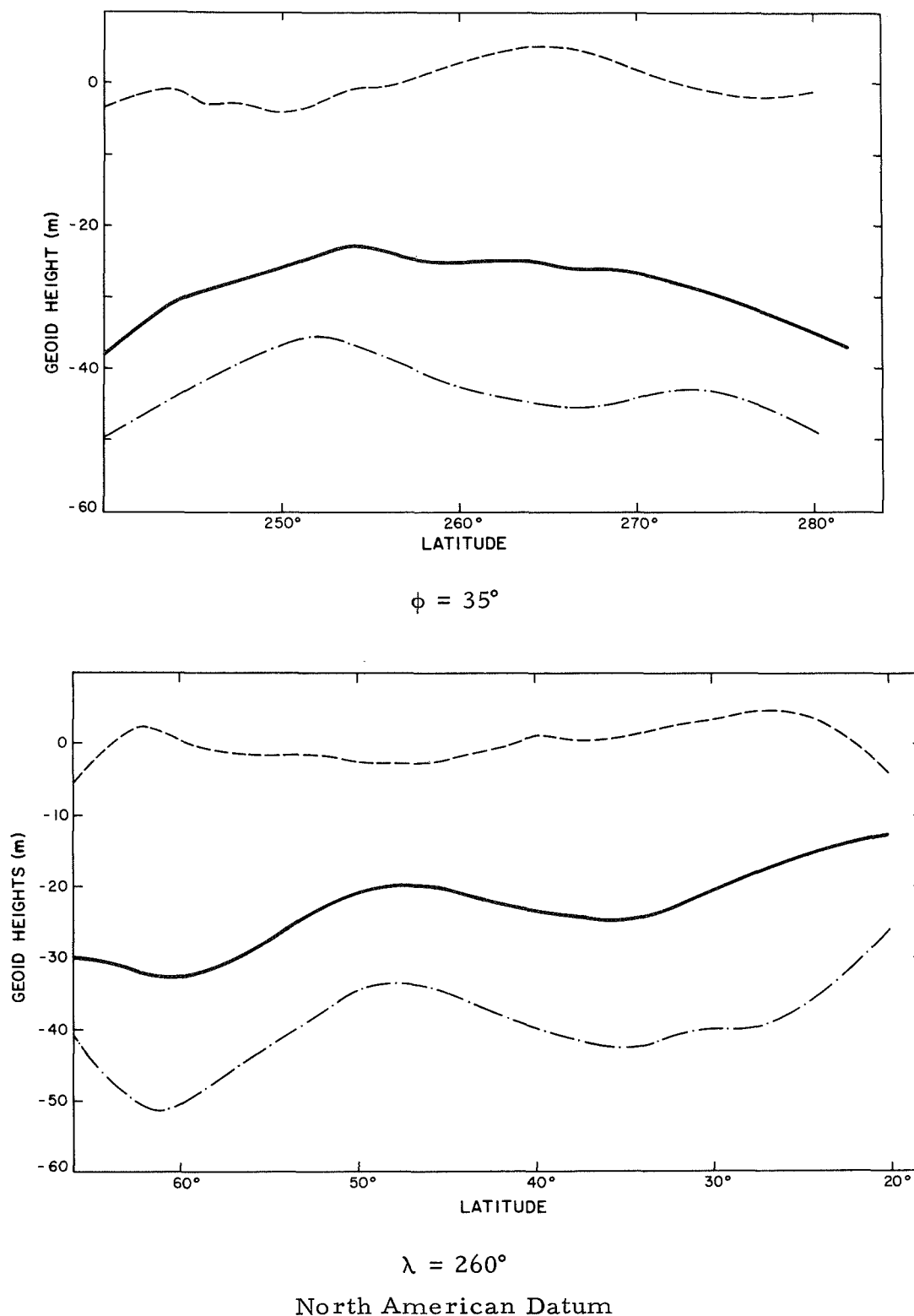
Fig. 7. Comparisons between geoid profiles obtained from the combination solution (solid lines) with profiles obtained from astrogeodetic measurements transformed into the global reference system (dashed lines). The difference between the two profiles, after the systematic part has been subtracted, is indicated by the dotted line.
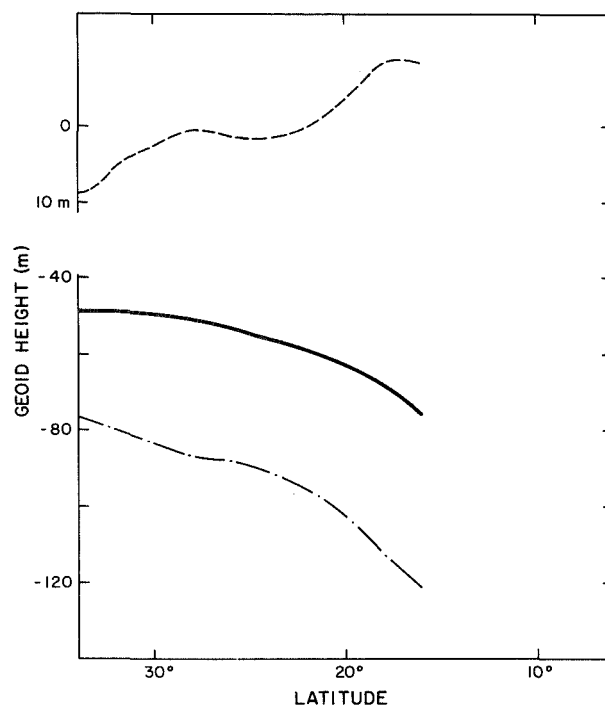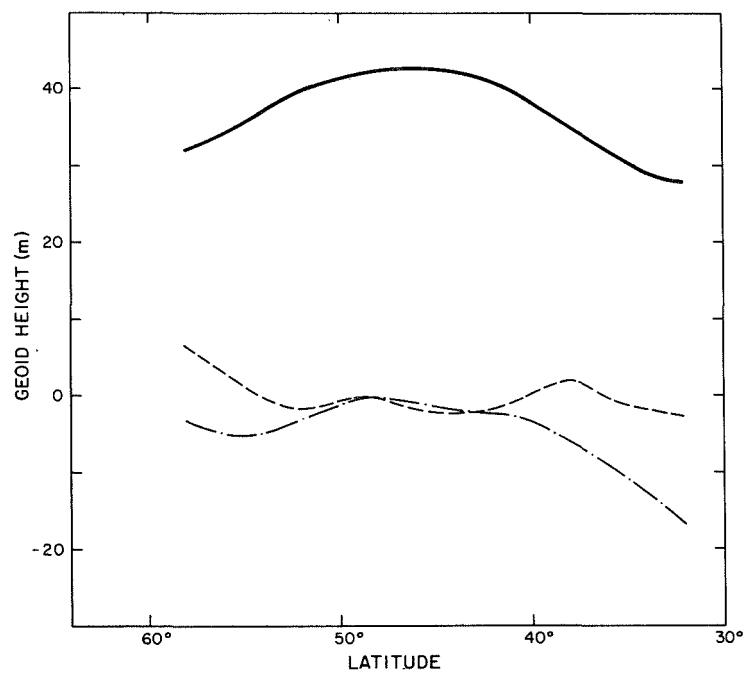
24
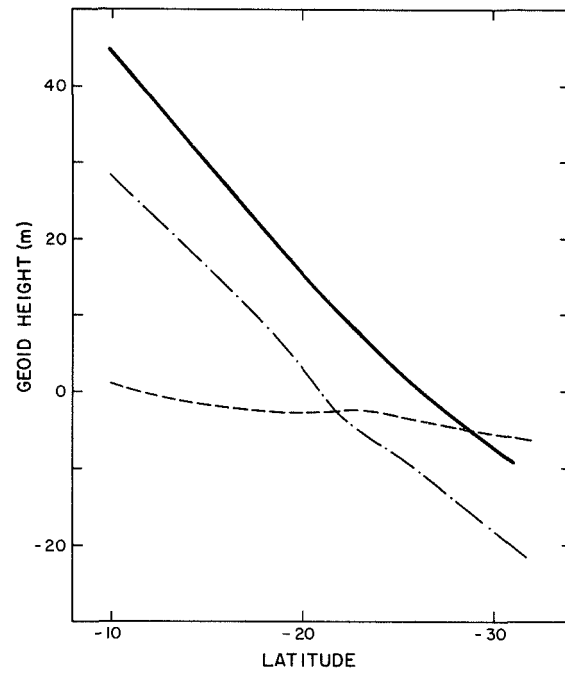
$\lambda = 136°25$
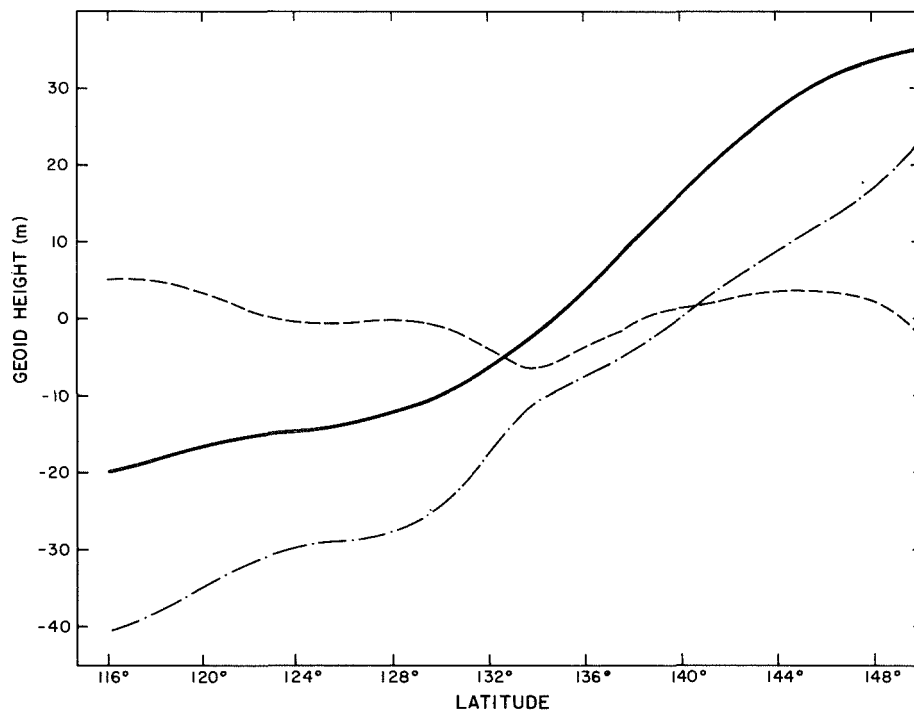
$\phi = -28°75$

Australian Geodetic Datum

Fig. 7 (Cont.)

$\lambda = 75°$

Indian Datum

$\lambda = 16°$

European Datum

Fig. 7 (Cont.)

26

TABLE 9. Summary of the comparisons between the geoid profiles obtained from the combination solution and the astrogeoids referred to the geocentric system. $\overline{\Delta h}$ is the systematic height difference between the profiles, $\sigma^2_{\delta h}$ the variance of the difference between the two profiles, σ^2_a the variance of the astrogeoid heights, and σ^2_S the contribution of the combination solution to $\sigma^2_{\delta h}$.

Datum	Profile	$\overline{\Delta h}$	$\sigma^2_{\delta h}$	σ^2_a	$\sigma^2_S = \sigma^2_{\delta h} - \sigma^2_a$
NAD	$\phi = 35°$	-15	8	1.5	6.5
NAD	$\lambda = 260°$	-16	6	1.5	4.5
AGD	$\phi = -28°75$	-12	10	1.5	8.5
AGD	$\lambda = 136°25$	-12	12	1.5	10.5
IND	$\lambda = 75°$	-36	30	1.5	28.5
EUR	$\lambda = 16°$	-42	6	1.5	4.5

$$(\sigma^2_S)_{AV} = 10.5 \ m^2$$

TABLE 10. Power spectra of free-air gravity anomalies.

Degree	Degree Variance (mgal^2)		
	Gravimetric Solution	Satellite Solution	Combination Solution
0	2.9		
1	-0.2		
2	5.9	7.4	7.4
3	31.0	33.3	33.0
4	18.2	19.7	20.0
5	7.3	17.5	17.8
6	20.7	14.4	15.7
7	9.2	16.4	15.5
8	7.0	8.5	6.7
9	8.7	15.1	12.7
10	9.4	17.7	12.9
11	5.7	13.7	12.2
12	3.5	8.4	5.1
13	7.0		11.1
14	9.4		8.4
15	9.9		13.2
16	5.5		13.8
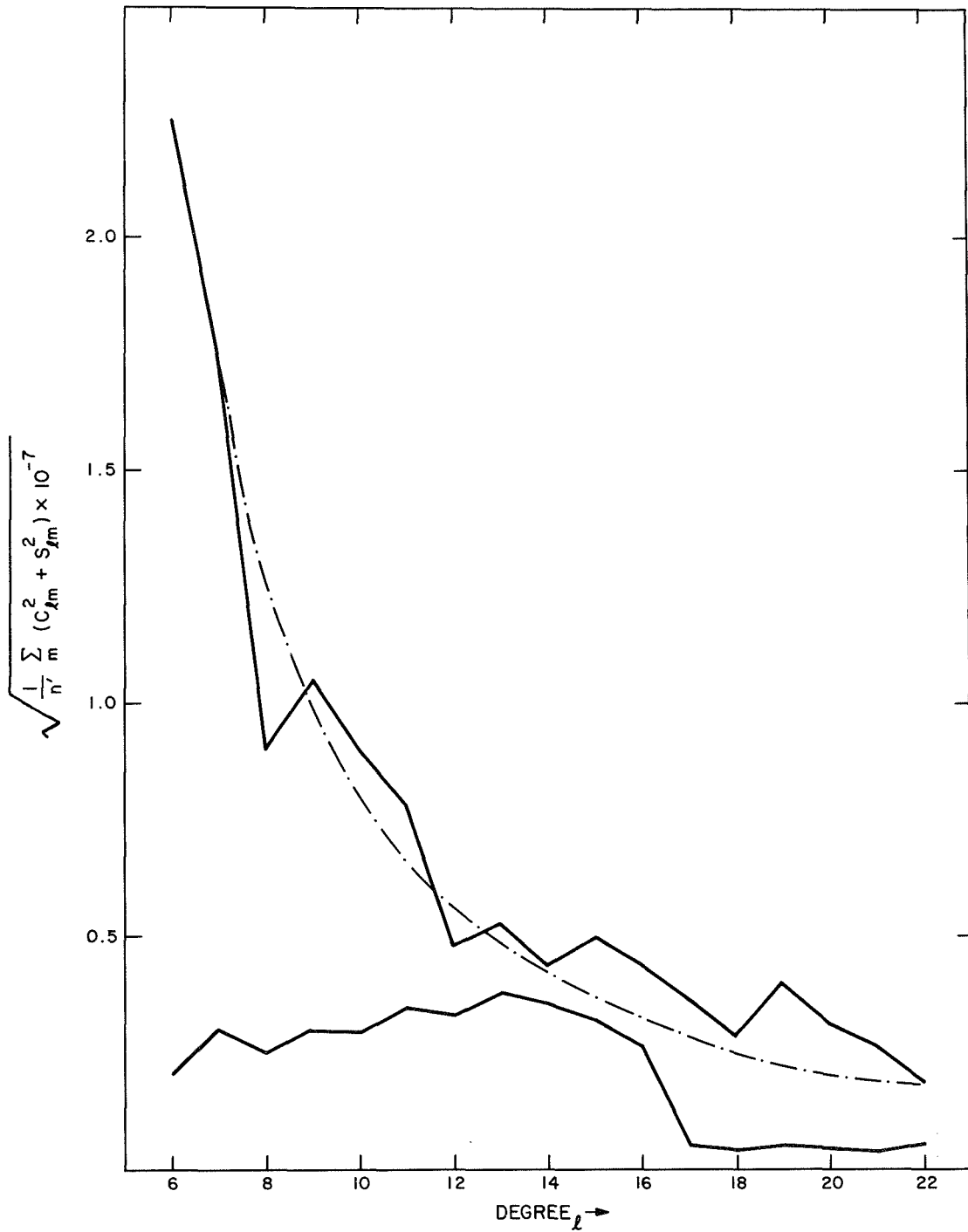
Fig. 8. Degree variances for $6 < \ell < 22$ for the combination solution.
Kaula's rule of thumb is indicated by the dashed line. For $2 < \ell < 6$ the degree
variances are in complete agreement with this rule. The lower curve gives
the degree variances corresponding to the precision estimates of the har-
monics, i.e., $1/n' \sum_m \left(\sigma^2_{C_{\ell m}} + \sigma^2_{S_{\ell m}} \right)$.

may be that the real earth actually has an attenuated power spectrum between $\ell = 20$ and the point where anomalies of 150 to 50 km become important ($\ell = 100$ to 300).

COMPARISON WITH GLOBAL TECTONICS

In one sense, a determination of the geophysical significance of the gravity field is a confirmation of the field, and in another, it is the raison d'être for the analysis. Although the following discussion is oriented toward the latter, it should be remembered that by having sorted out the geophysical implications of the gravity field, both results have been verified.

Figure 9 is a plot of free-air anomalies, referred to the figure of hydrostatic equilibrium (an ellipsoid of flattening 1/299.8), in accord with the explanation of Goldreich and Toomre (1969) for the excess oblateness.

There are two major effects of the new data:

A. The improved resolution results in the breakup of the two largest features in the southern oceans. The large area of mild anomaly in the South Pacific is now resolved into two negative areas with a positive area between, the former over basins and the latter along the East Pacific Rise. In the area between Africa and Antarctica, a single large positive feature centered in the "vee" between the two rises is now divided into two positive features over the rises and an area of mild anomaly between. In general, most of the vigorous ocean rises are now positives, rather than "mild" features.

B. The use of the hydrostatic flattening results in the intensification of the negative anomalies in the glaciated areas near the poles: to an extent at the South Pole, which is much greater than can be imputed to glacial loading.

Lesser effects are the appearance of the highest Himalayas as a small positive belt; the removal of the overlap of the ocean rise by the South Australian basin negative; the emphasis of the positive belt from the
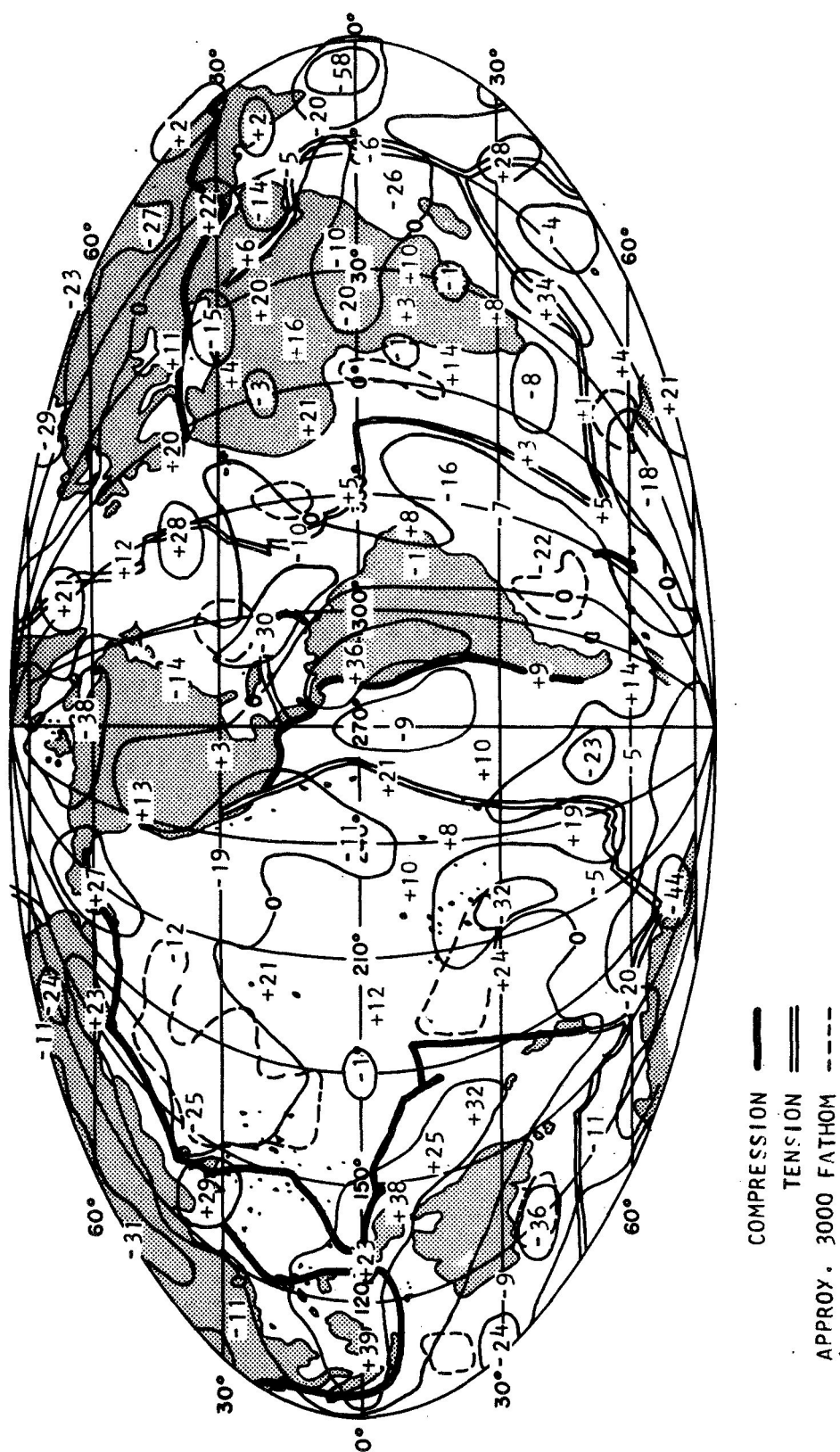
30

Fig. 9. Free-air anomalies in milligals referred to an ellipsoid of flattening 1/299.8. Calculated from the spherical-harmonic coefficients of the gravitational field of degrees 2 through 16 of Gaposchkin and Lambeck (1970). (Nonzero contours enclosing only one value have been omitted on all figures.) Global tectonic lines of compression and tension from Isacks, Oliver, and Sykes (1968), and major basins indicated by approximate 3000-fathom line on all figures.

COMPRESSION ▬▬▬
TENSION ▬▬
APPROX. 3000 FATHOM ▬ ▬ ▬

31

Carpathians to Iran; the reduction of the East Mediterranean negative; and the reduction or removal of positive features in areas of slight recent tectonic activity in northeast USSR, the Central Pacific, and Australia.

Figure 10 is the corresponding isostatic anomaly map, using the spherical harmonic expansion of the Airy-Heiskanen 30-km crust isostatic correction calculated by Uotila (1962). As anticipated, oceanic maxima and continental minima are enhanced in the isostatic map.

As previously pointed out (Kaula, 1967), the correlation of gravity with topography is poor for the fifth and lower degrees. On the other hand, Hide and Malin (1970) have recently shown that the low-degree harmonics of the gravity field have a high correlation with the corresponding harmonics of the magnetic field, provided the latter is rotated 160° eastward. The obvious application for the purpose of interpreting upper mantle and crustal phenomena is to use a residual field. Figure 11 is the free-air anomaly field calculated from spherical harmonic coefficients of degrees 6 through 16, and Figure 12 is the corresponding isostatic anomaly field. In the four successive representations of Figures 9 through 12, the correlation of ocean rises with positive anomalies appears more and more emphasized.

As discussed in Kaula (1969), it seems appropriate to analyze the gravity field in terms of reasonably contiguous blocks of anomaly X area, since, by the half-space application of Gauss's theorem, this quantity is directly proportional to excess mass, which in turn is a primary measure of the stresses required. Table 11 gives the 30 largest blocks in terms of free-air anomalies referred to the hydrostatic figure, while Table 12 gives the 25 largest blocks in terms of isostatic anomalies referred to the fifth-degree figure. Of the 12 question marks in Table 4 of Kaula (1969), about 10 seem to be resolved. The greatest question remaining is the great negative over Antarctica; it is too large by more than a factor of 3 to be attributable to the loss of ice in recent geologic time (O'Connell, 1970).

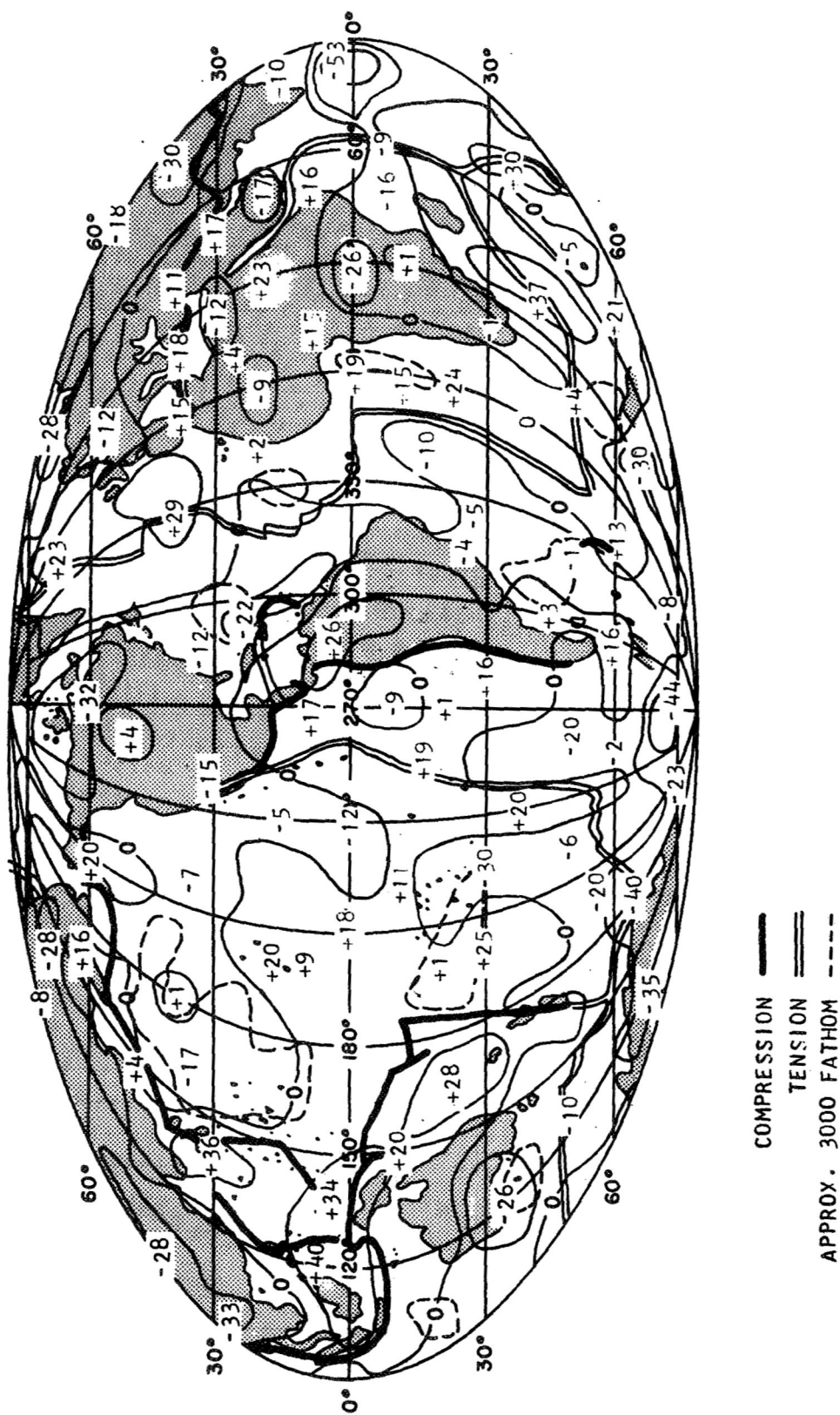The types given in Tables 11 and 12 are those used in Kaula (1969), with some obvious modifications.

32

Fig. 10. Isostatic anomalies in milligals referred to an ellipsoid of flattening 1/299.8. Airy—Heiskanen compensation with nominal crustal thickness of 30 km. Calculated from Figure 9, less the spherical-harmonic coefficients for the isostatic correction of degrees 2 through 16 of Uotila (1962).
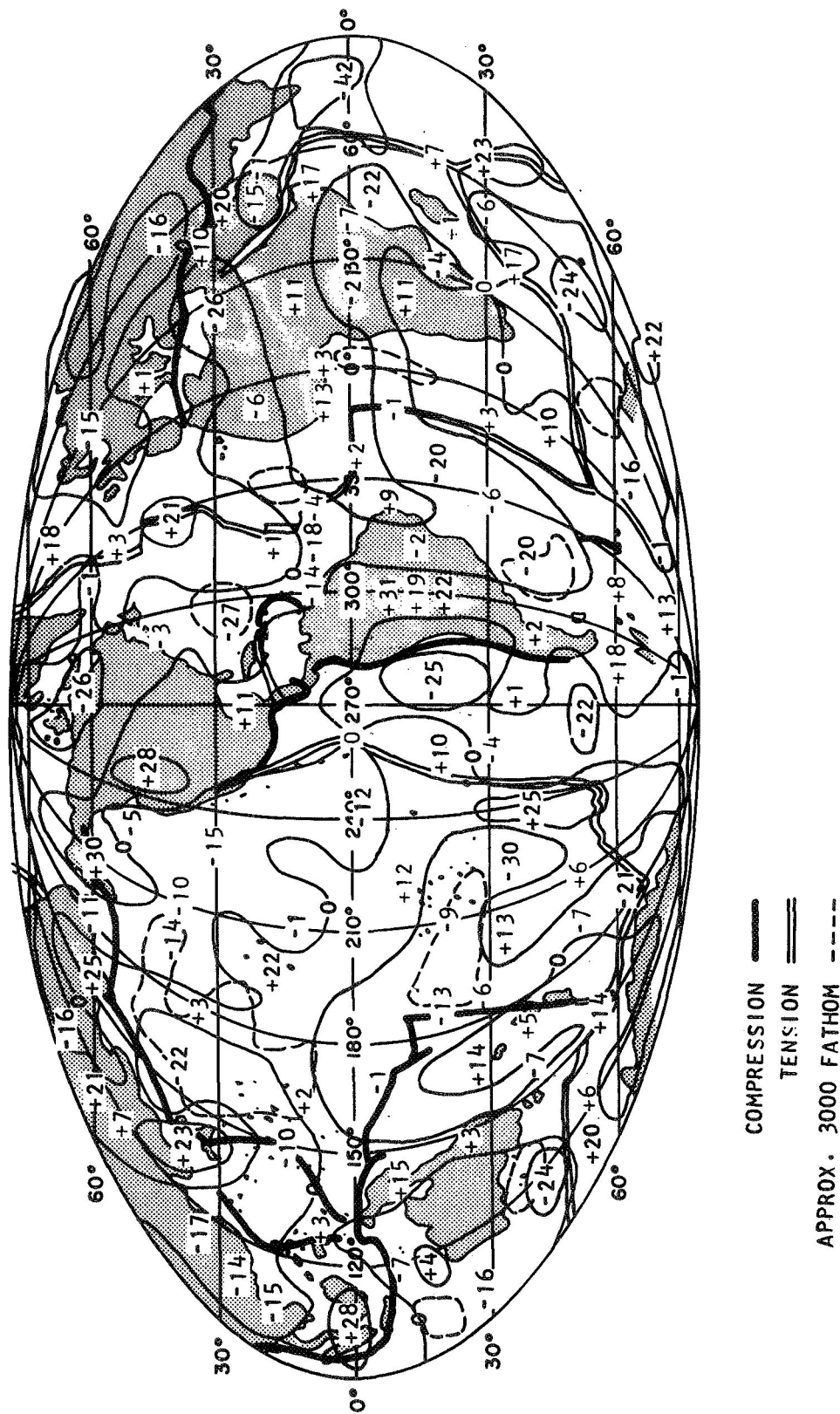
Fig. 11. Free-air anomalies in milligals referred to a fifth-degree figure. Calculated from the spherical-harmonic coefficients of the gravitational field of degrees 6 through 16 of Gaposchkin and Lambeck (1970).

34
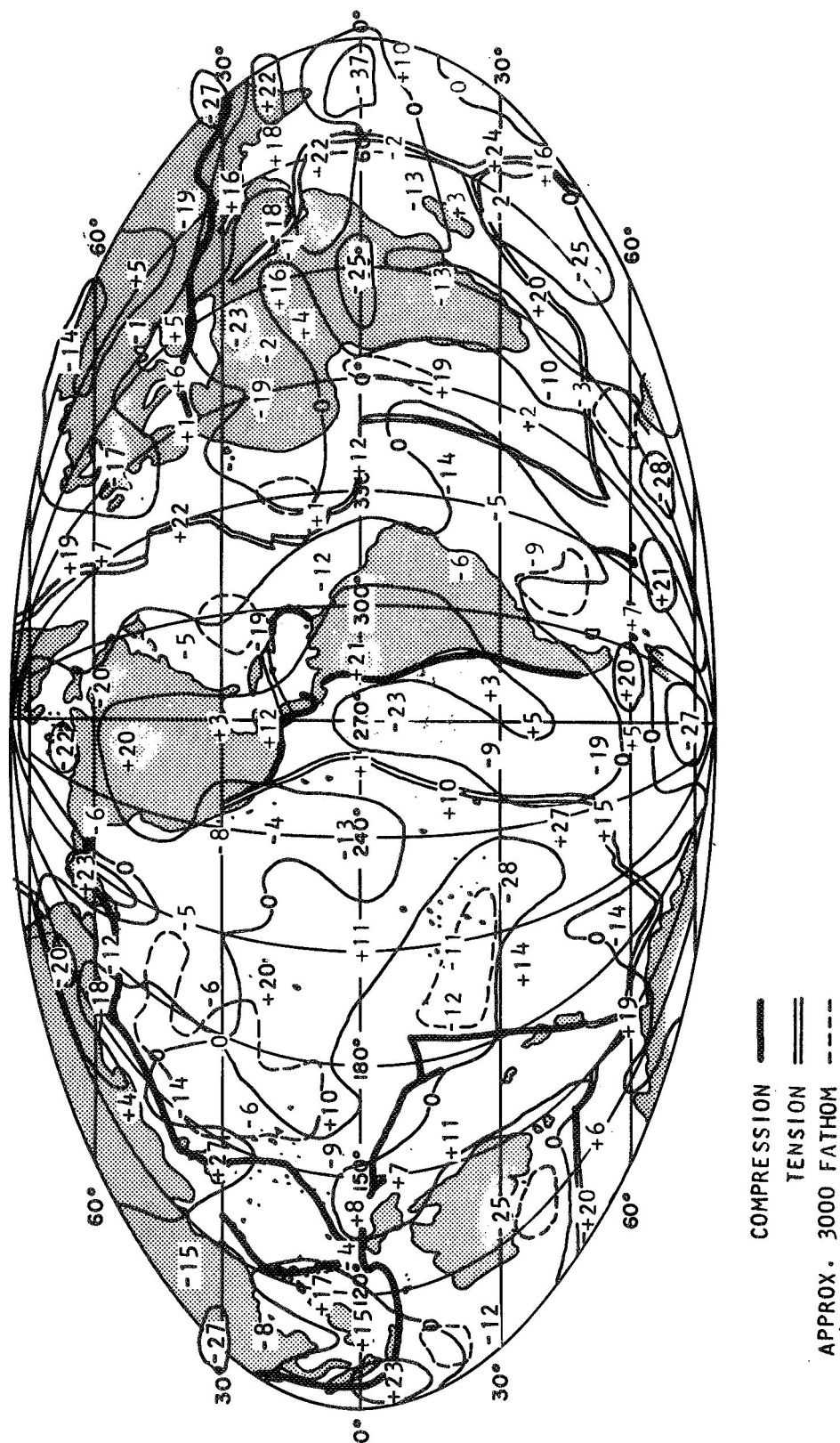
Fig. 12. Isostatic anomalies in milligals referred to a fifth-degree figure. From Figure 11, less the spherical-harmonic coefficients for the isostatic correction of degrees 6 through 16 of Uotila (1962).

COMPRESSION
TENSION
APPROX. 3000 FATHOM

TABLE 11. Areas of exceptional gravity anomaly, defined as having an area × free-air anomaly referred to the hydrostatic figure of more than 50 mgal × 10^6 km^2 ($1.17 × 10^{21}$ g) in absolute magnitude and an absolute anomaly of more than 10 mgal throughout the area.

General Location	Area (10^6 km^2)	Free-Air Anomaly × Area (mgal × 10^6 km^2)	Mean Free-Air Anomaly (mgal)	Type
A. Positive Features				
1. Sumatra–Philippines–Solomons	18.9	461	27	Arc
2. Andes–West Amazon Basin	9.4	206	22	Arc-Orogenic
3. Solomons–Tonga–Kermandec	10.4	178	17	Arc
4. Mid-Indian Rise–Indian–Antarctic Rise	9.4	175	19	Rise
5. Crozet Plateau–South Madagascar Rise	6.3	117	19	Rise
6. Mexico–Northwest Colombia	7.3	107	15	Arc
7. Carpathians–Turkey–Iran	7.2	103	14	Orogenic
8. Hawaii	6.1	96	16	Shield
9. Azores Plateau	5.8	95	16	Rise
10. Japan–Bonins	4.6	92	20	Arc
11. Atlas–Iberia–West Mediterranean	5.5	86	16	Arc-Orogenic
12. West Africa–Guinea Basin	6.2	85	14	Orogenic
13. Ahaggar–Tibesti–Nigeria	4.7	77	16	Orogenic
14. Greenland–Iceland–Norwegian Sea	4.6	76	16	Rise
15. East Pacific Rise, North of Easter Island	4.2	64	15	Rise
16. Walvis Rise–Southwest Africa	4.5	58	13	Rise
B. Negative Features				
1. Antarctica	22.4	-511	-23	Glac.-Basin?
2. Siberian Plateau–Turkestan–Himalayas	15.1	-289	-19	Glac.-Orogenic
3. North Canada	10.1	-218	-22	Glaciated
4. North American–Guiana Basins	11.7	-212	-18	Basin
5. Somali Basin–Central Indian Ocean	6.2	-193	-31	Basin
6. North Pacific Basin–Northeast Pacific Slope	12.3	-175	-14	Basin
7. West Australian Shield–South Australian Basin	4.6	-121	-26	Basin
8. Northwest Pacific Basin	5.3	-116	-22	Basin
9. Wharton Basin	5.6	- 98	-17	Basin
10. Northwest Siberia–Aleutian Basin	5.6	- 87	-16	Glac.-Basin
11. Society Island–Southwest Pacific Basin	3.2	- 69	-22	Basin
12. Congo–Kenya	5.0	- 60	-12	Basin-Rift
13. Argentine Basin	3.6	- 54	-15	Basin
14. Chile Rise–Pacific Antarctic Basin	2.8	- 50	-18	Basin

TABLE 12. Areas of exceptional gravity anomaly, defined as having an area × isostatic anomaly referred to a fifth-degree figure of more than 50 mgal × 10^6 km^2 (1.17×10^{21} g) in absolute magnitude and an absolute anomaly of more than 10 mgal throughout the area.

General Location	Area (10^6 km^2)	Isostatic Anomaly × Area (mgal × 10^6 km^2)	Mean Isostatic Anomaly (mgal)	Type
A. Positive Features				
1. Southeast Pacific Rise	6.6	135	20	Rise
2. Mid-Indian-Amsterdam-Naturaliste Ridge	6.1	100	16	Rise
3. Borneo-Sumatra-Cocos	5.3	98	18	Arc
4. Indian Peninsula-Bay of Bengal	4.7	82	17	Sediment?
5. Southeast Indian, MacQuarrie Rises	5.1	76	15	Rise
6. North Atlantic-Arctic Ocean	7.1	73	10	Glaciated(?) Rise
7. Azores Plateau	4.7	73	16	Rise
8. Indian-Antarctic, Gaussberg Ridges	4.5	72	16	Rise
9. North Andes-West Amazon Basin	5.0	72	14	Arc-Orogenic
10. Northeast Georgia-South Sandwiches-Mid-Atlantic	4.3	68	16	Rise-Arc
11. Japan-Bonins	4.0	66	16	Arc
12. Carlsberg Ridge-Gulf of Aden	3.7	65	18	Rise
13. South Alaska	3.6	65	18	Arc-Orogenic
14. Walvis Rise	4.5	61	14	Rise
B. Negative Features				
1. Himalayas-China	8.0	-141	-18	Orogenic
2. Antarctica	8.1	-140	-17	Glaciated Basin?
3. Laccadives-Ceylon-Mid-Indian Ocean	5.0	-130	-26	Basin?
4. North Canada-Greenland	7.5	-123	-16	Glaciated
5. Australian Shield-South Australian Basin	7.7	-113	-15	Basin
6. North American-Guiana-Parnaiba Basins	7.3	-96	-13	Basin
7. Galapagos-Peru Basin	6.1	-96	-16	Basin
8. Society-Tuamotu-Australian Sea Mt.	6.8	-96	-14	Basin?
9. Congo-Kenya	3.7	-74	-20	Basin-Rift
10. East Crozet Basin-Kerguelen	2.6	-53	-20	Basin
11. Northwest Europe	3.5	-51	-15	Glaciated

INTERPRETATION

The principal inference from the large areas of postglacial uplift is, of course, the asthenosphere — a relatively plastic layer in the upper mantle, 80 to 400 km or more deep. Of the seven or eight major feature types, the glaciated areas are alone in being <u>transient</u>, with a decay time on the order of a few thousand years (O'Connell, 1970).

Since the lithosphere is not capable of supporting elastically the necessary stresses for features thousands of kilometers in extent (McKenzie, 1967), the other broad departures in the earth from equilibrium must entail flow in the asthenosphere. However, the asthenosphere is stiff enough, and the thermal conductivity of the earth poor enough (i. e., the Prandtl number is large), that it is generally agreed that the flow is essentially <u>steady state</u> (Turcotte and Oxburgh, 1967, 1969). As indicated by magnetic reversal patterns, the present pattern of tectonic motion has persisted for about 10 million years (Heirtzler, Dickson, Herron, Pitman, and Le Pichon, 1968).

In a steady-state flow system, for a mass excess in a particular region to be maintained, there must be effectively a deceleration in the Lagrangian sense of matter entering the region and an acceleration of matter leaving it; the converse must apply to a region of mass deficiency. Since the compressibility of upper mantle material is slight, these "decelerations" must be accomplished by 1) the piling up of material at the surface, 2) the replacement of less dense by more dense material at an interior interface, 3) thermal contraction, 4) transition to a denser phase, or 5) petrological fractionation in which a less dense component is left behind. The reverse of one or more of these processes is needed to accomplish an "acceleration."

If the asthenosphere is a relatively thin layer, then the obvious direction to transfer matter so as to affect the external gravitational field is lateral. However, vertical transfers are not to be ruled out: an upward displacement of material making the density higher than the average at a shallow level, balanced by a mass deficiency at considerable depth (say below 200 km), could

account for a gravity excess. From the formula for the potential arising from a spherical-harmonic surface distribution of mass (Kaula, 1968, p. 67) we have, for a mass excess of $\Delta\rho h$ of width L compensated at depth d,

$$\Delta g \approx 2\pi^2 G\frac{d}{L}\Delta\rho h \quad .$$

But then to say the data are satisfied by isostatic compensation at great depth is to beg the question as to the response of the asthenosphere to the stresses that must necessarily exist at the intervening levels.

The relationship of gravity anomalies to the flow system depends drastically on the boundary conditions. In a system of thermal convection, if the boundary is fixed, an upcurrent is associated with a negative anomaly, because of its lower density (Runcorn, 1965). But if the boundary is free, an upcurrent is associated with a positive anomaly because the effect of the mass pushed up at the surface outweighs the density effect (Pekeris, 1935; McKenzie, 1968).

In the case of the real earth, the question becomes to what extent the lithosphere (the layer of relative strength) and the crust (the lower density, uppermost layer of the lithosphere) act as part of the convective flow and to what extent they act as a restraining boundary to the flow. Manifestly, they act both roles to differing degrees in different parts of the earth. The lithosphere can even be simultaneously a fixed boundary for horizontal forces, in being able to act as a rigid plate in tectonic motions, and a free boundary for vertical forces, in not resisting convective upthrusts. The extent to which a particular portion of the lithosphere acts as a free or fixed boundary depends on its temperature, size of feature, rate of motion of material into and out of a feature, and composition (in particular, its water content). The situation may be further complicated by steady surface transfers of matter — i. e., erosion and sedimentation.

39

How a boundary acts in the range between perfectly free and perfectly fixed depends on both 1) its elastic properties — its rigidity and thickness, and 2) its plastic properties — most simply expressed as a decay time in response to a transient loading, dependent on the dimensions of the loading and stress as well as on the creep properties of the material. Under small stresses, the decay time of the lithosphere is very long: it is effectively acting as an elastic layer in areas of postglacial uplift. But under greater stresses, such as in the major areas of mass excess, the notion of decay time is complicated by the nonlinear dependence of strain rate on stress (Weertman, 1970), as manifested by the seismicity of these regions. Qualitatively, for both elastic and plastic behavior, we should expect that the thicker, the colder, the less hydrous the lithosphere is in a particular region, the more it will behave like a fixed boundary. But quantitatively, we should expect that in some cases it may be difficult even to infer the correct sign of the gravity anomaly.

The flow system for a body with boundaries that are partly fixed and partly free would be a difficult problem to treat rigorously. However, we might expect that usually the nature of the local boundary conditions would predominate in determining the characteristics of a particular region. We shall apply this assumption in the analysis of feature types below.

In Kaula (1969), 11 gravity-anomaly area types were proposed, 6 of which appeared to be associated with current internal activity in the earth. We shall discuss these six (somewhat modified) in an order suggested by their apparent relationship to the global-tectonic pattern: 1) active ocean rises, 2) oceanic shield basalts still active in Quaternary, 3) basins, 4) trench and island arcs currently active, 5) current orogeny without extrusives, and 6) Cenozoic orogeny with extrusives in Quaternary.

Active Ocean Rises. The indication from the new data that these areas are generally of positive gravity anomaly is consistent with their being free boundaries over upcurrents in a convective system. Their well-known characteristics of high heat flow, shallow depth in the ocean, thin sediments,

40

large-scale volcanism, frequent moderate earthquakes, lack of a distinct Moho, and prevalence of intermediate seismic primary velocities in the range 7.2 to 7.7 km/sec are generally taken to indicate that the rises are the sites of upwelling and spreading out in a convective cycle. The intensity and uniformity of heating is apparently sufficient to prevent this mass imbalance from being large. Such small temperature gradients are the expected consequence of a strong temperature dependence of viscosity (Tozer, 1967; Turcotte and Oxburgh, 1969).

Oceanic Shield Basalts. With the improved data, all major oceanic positive areas appear to be associated with spreading centers except one — Hawaii. Hawaii appears to be the buildup of an appreciable mass excess by extrusive activity off the rise. This buildup is in spite of a sinking of the crust, as pointed out by Menard (1969). An approach to isostatic adjustment is also suggested by depths to the Moho somewhat greater than the oceanic average (Drake and Nafe, 1968). But apparently the lithosphere has cooled sufficiently to cause a lag in the attainment of equilibrium. This notion is corroborated by the relatively low heat flow. The existence of such a feature indicates that the asthenospheric flows that generate the required pressure do not necessarily have a simple and direct relationship to the lithospheric plate motions (McKenzie, 1969).

Basins. This commonest of the major features always occurs some-where to the flanks of ocean rises. However, landward of the basin may be a trench and island arc, an orogenic belt, or a relatively quiescent continent on the same tectonic plate. This suggests that the nature of the flows associated with basins depends more on where the material came from than where it is going.

The direct cause of the negative isostatic anomaly is most likely that the crust carried along in the sea-floor spreading is thicker than compatible with the depth of the basin; a Moho deeper by less than a kilometer is adequate to account for the average isostatic anomaly of -14 mgal.

The real problem, of course, is what is the nature of the asthenospheric withdrawal that causes the 3-km drop from the rise to the basin. Such a drop could be caused by a downcurrent component in the convective system resulting from the settling out of denser components. Such settling out would be expected in a laterally moving flow that was cooling. But a 3-km drop requires much more than thermal contraction; furthermore, if there is an appreciable negative anomaly as well, the settling out cannot just be immediately below the basin lithosphere but must be either 1) at a depth of several hundred kilometers below the basin, or 2) between the ocean rise and the basin. Process 1) could be effected by the phase transitions of olivine and pyroxene, which occur at depths of 300 to 600 km, while process 2) might be facilitated by gabbro-to-eclogite transitions at shallower depths.

The sharpness of the crust-mantle boundary, with the 7.2- to 7.7-km/sec gap in velocities (Drake and Nafe, 1968), makes it impossible for the crust to be directly involved in causing the negative anomaly. But if the crust is being carried passively along — as suggested by the lack of seismicity, volcanism, or disturbance of the sea floor — then it is hard to understand why it is thicker under the basins than it is on the flanks of the rises, as emphasized by Le Pichon (1969). Could it be that consolidated sediments are mistaken for basement rock? Sedimentation itself is a secondary process in explaining the gravity-anomaly pattern, more a result than a cause: if the thick sediments are the driving force, then the isostatic anomalies in ocean basins would be positive, rather than negative.

Possibly to be included in the category of basins caused by the behavior of the lithosphere as a free-boundary overflow with settling out of denser components are two land features, Antarctica and the Congo Basin. Antarctica is an extremely large feature — large enough to require a unique explanation.

Trench and Island Arcs. The now generally accepted model of McKenzie (1969) and others of a colder, denser oceanic lithospheric slab being thrust down under a less dense but stiffer continental margin fits a simple notion

42

of the gravity pattern: the dominant feature is the broad positive anomaly associated with the denser downthrust slab, while the secondary feature is the narrow negative belt associated with the trench caused by tensile cracking and the downward-breaking line. But this simple picture is based on the assumption that the applicable boundary condition of the convective flow is more "fixed" than "free": in other words, the time scale of the process is short enough that the strength of the continental lithosphere (and perhaps the oceanic lithosphere as well) significantly resists being pulled down by the downcurrent. This general idea that resistance to flow is necessary to make positive gravity anomalies of densifications applies not only to the boundary layer but also to deeper strata: the downthrust slab could in part be supported by stiffer matter below the asthenosphere, as suggested by Isacks and Molnar (1969) and others from seismic data.

The association of the downthrust slab with positive anomalies also suggests that the driving force is a push from above rather than withdrawal from below. Whether this "push" is the gravitationally caused sinking of the denser oceanic lithosphere, the pressure of the spreading sea floor behind it, or the viscous drag by the sublithospheric flow does not seem resolvable from the gravity data.

Current Orogeny without Extrusives. The hypothesis of McKenzie (1969) that purely continent vs. continent compression results in folding rather than in downthrust because of the excessive buoyancy of the thicker crust is appealing as an explanation for the strongly negative gravity anomalies associated with the Asian part of the Alpide belt. The resulting pileup of lower density material results in a mass deficiency in the short run, because the stiffness of the lithosphere containing low-density crust enables it to push out of the way higher density asthenospheric material. But in the longer run, the trend from "fixed" to "free" boundaries is expressed by the forcing upward of the lithosphere; geologic and geodetic indications are that the Himalayas—Turkestan complex is currently rising (Gansser, 1964; Artyushkov and Mescherikov, 1969).

The thick layers of sedimentary and metamorphic rocks constituting the upper part of the Himalayas have existed since pre-Cambrian times, and hence the excess heat generation and thermal blanketing may influence the situation. Furthermore, there may be a contribution from erosion, as corroborated by the positive features over the Bay of Bengal and the Arabian Sea, which appear most strongly in Figure 12.

Cenozoic Orogeny with Extrusives. These mountain-building areas, listed as orogenic among the positive features in Table 11, seem to require less explanation in that they are of more limited extent and are closer to isostatic equilibrium. Most are associated with compressive belts of the global tectonic system, but this is not entirely so. Why they differ from the Himalayas—Turkestan complex in being positive may be the lack of the preexisting great thicknesses of sedimentary and metamorphic rocks, or it may be the presence of oceanic crust to be consumed (McKenzie, 1970). They may also be the continental equivalents of Hawaii to some extent: the coincidence of weak features in the lithsophere with regions of excess pressure and heat in a convective system that is not directly related to surface features. Most of these areas have positive seismic-delay residuals, suggesting high temperatures to considerable depth.

DISCUSSION AND CONCLUSIONS

The gravity data now appear to confirm rather well the dependence of plate tectonics on mantle convection inferred from other phenomena associated with the midocean rises and the compressive belts (Isacks, Oliver, and Sykes, 1968). The principal respect in which this picture is enhanced is the inference that ocean basins are associated with significant down-currents entailing settling out of denser components and, probably, phase transitions. That this process results in negative gravity anomalies depends on the time scale of the effect being long enough that the lithosphere is of negligible strength and hence acts like a free boundary.

The greatest feature not readily related to the global tectonic system is the Antarctic negative, much too large to be explained by glacial melting. Antarctica is almost surrounded by ocean rises. Hence, either these rises are migrating away from Antarctica, or Antarctica is a sink. The latter seems implausible, since there is none of the seismicity expected with the destruction or folding of the lithosphere: it is difficult for Antarctica to pass on the lithosphere to some other area, as do the ocean basins.

Other features not well explained by the global tectonic pattern are the gravity excesses associated with extrusive flows away from the ocean rises and trench and island arcs, in both oceanic and continental areas. Both these features appear to require higher temperatures in the asthenosphere generating excess pressures, together with weaknesses in the lithosphere allowing the extrusions. It is, however, difficult to choose whether the resulting net mass excess is a consequence of sufficient overall strength in the lithosphere to support the extruded load or of behavior as a free boundary over an upcurrent: perhaps a partial current that is the upward motion of a less dense component, the reverse of the process that appears necessary to account for the ocean basins.

Anticipated properties of the mantle-convective system that need to be better related to the gravity field are the stress dependence and temperature dependence of the effective viscosity, the horizontal temperature gradients arising from variations in radiogenic heating, and the contributions to driving the system by fractionations and phase transitions. All these properties are important, of course, to the solution of the entire global tectonic problem.

ACKNOWLEDGMENTS

Ethiopia

    Haile Selassie I University

Hawaii

    University of Hawaii

    Institute for Astronomy

    Institute of Geophysics

Iran

    Université de Teheran
    Institute Géophysique

Netherlands Antilles

    Curaçao Welfare Bureau

Peru

    Instituto Geofisico del Peru

    Universidad Nacional de San Agustin

South Africa

    Council for Scientific and Industrial Research

Spain

    Instituto y Observatorio de Marina

REFERENCES

Artyushkov, E. V., and Mescherikov, Yu. A., Recent movements of the earth's crust and isostatic compensation, in The Earth's Crust and Upper Mantle, AGU Monog. 13, edited by P. J. Hart, 379-390, 1969.

Drake, C. L., and Nafe, J. E., The transition from ocean to continent from seismic refraction data, in The Crust and Upper Mantle of the Pacific Area, AGU Monog. 15, edited by L. Knopoff, C. L. Drake, and P. J. Hart, 174-186, 1968.

Gansser, A., Geology of the Himalayas, John Wiley & Sons, Inc., Interscience Publ., London, 289 pp., 1964.

Gaposchkin, E. M., A dynamical solution for the tesseral harmonics of the geopotential and station coordinates using Baker-Nunn data, in Space Research VII, edited by R. L. Smith-Rose, S. A. Bowhill, and J. W. King, North-Holland Publ. Co., Amsterdam, 683-693, 1967.

Gaposchkin, E. M., and Lambeck, K., 1969 Smithsonian Standard Earth (II), Smithsonian Astrophys. Obs. Spec. Rep. No. 315, 93 pp., 1970.

Goldreich, P., and Toomre, A., Some remarks on polar wandering, J. Geophys. Res., 74, 2555-2567, 1969.

Heirtzler, J. R., Dickson, G. O., Herron, E. M., Pitman, W. C., III, and Le Pichon, X., Marine magnetic anomalies, geomagnetic field reversals, and motions of the ocean floor and continents, J. Geophys. Res., 73, 2119-2136, 1968.

Hide, R., and Malin, S. R. C., Novel correlations between global features of the earth's gravitational and magnetic fields, Nature, 225, 605-609, 1970.

Isacks, B., Oliver, J., and Sykes, L. R., Seismology and the new global tectonics, J. Geophys. Res., 73, 5855-5899, 1968.

Isacks, B., and Molnar, P., Mantle earthquake mechanisms and the sinking of the lithosphere, Nature, 223, 1121-1124, 1969.

Kaula, W. M., Test and combination of satellite determinations of the gravity field with gravimetry, J. Geophys. Res., 71, 5303-5314, 1966.

Kaula, W. M., Geophysical implications of satellite determinations of the earth's gravitational field, Space Sci. Rev., 7, 769-794, 1967.

Kaula, W. M., An Introduction to Planetary Physics: the Terrestrial Planets, John Wiley & Sons, Inc., New York, 490 pp., 1968.

Kaula, W. M., A tectonic classification of the main features of the earth's gravitational field, J. Geophys. Res., 74, 4807-4826, 1969.

Kaula, W. M., Chairman, The Terrestrial Environment: Solid-Earth and Ocean Physics, NASA Contractor Report CR-1579, 1970.

Köhnlein, W. J., Corrections to station coordinates and to nonzonal harmonics from Baker-Nunn observations, in Space Research VII, edited by R. L. Smith-Rose, S. A. Bowhill, and J. W. King, North-Holland Publ. Co., Amsterdam, 694-701, 1967a.

Köhnlein, W. J., The earth's gravitational field as derived from a combination of satellite data with gravity anomalies, Smithsonian Astrophys. Obs. Spec. Rep. No. 264, 57-72, 1967b.

Kozai, Y., Revised values for coefficients of zonal spherical harmonics in the geopotential, Smithsonian Astrophys. Obs. Spec. Rep. No. 295, 17 pp., 1969.

Lambeck, K., The relation of some geodetic datums to a global geocentric reference system, Bull. Géod., in press, 1970.

Le Pichon, X., Models and structure of the oceanic crust, Tectonophys., 7, 385-401, 1969.

Le Pichon, X., and Talwani, M., Regional gravity anomalies in the Indian Ocean, Deep Sea Res., 16, 263-274, 1969.

Lundquist, C. A., and Friedman, H. D., Eds., Scientific horizons from satellite tracking, Smithsonian Astrophys. Obs. Spec. Rep. No. 236, 250 pp., 1966.

Lundquist, C. A., and Veis, G., Eds., Geodetic parameters for a 1966 Smithsonian Institution Standard Earth, Smithsonian Astrophys. Obs. Spec. Rep. No. 200, 3 vol., 1966.

McKenzie, D. P., Some remarks on heat flow and gravity anomalies, J. Geophys. Res., 72, 6261-6273, 1967.

McKenzie, D. P. , The influence of the boundary conditions and rotation on convection in the earth's mantle, Geophys. J. Roy. Astron. Soc. , 15, 457-500, 1968.

McKenzie, D. P. , Speculations on the consequences and causes of plate motions, Geophys. J. Roy. Astron. Soc. , 18, 1-32, 1969.

McKenzie, D. P. , Plate tectonics of the Mediterranean region, Nature, 226, 239-243, 1970.

Menard, H. W. , Growth of drifting volcanoes, J. Geophys. Res. , 74, 4827-4837, 1969.

Mottinger, N. , Status of D. S. F. locations solution for deep space probe missions, Space Programs Summary No. 37-60, Jet Propulsion Laboratory, Pasadena, California, vol. II, 77-89, 1969.

O'Connell, R. J. , Pleistocene glaciation and the viscosity of the lower mantle, J. Geophys. Res. , 75, in press, 1970.

Pekeris, C. L. , Thermal convection in the interior of the earth, Mon. Not. Roy. Astron. Soc. Geophys. Suppl. , 3, 343-367, 1935.

Runcorn, S. K. , Changes in the convective pattern in the earth's mantle and continental drift: evidence for a cold origin of the earth, Phil. Trans. Roy. Soc. London A, 258, 228-251, 1965.

Talwani, M. , and Le Pichon, X. , Gravity field over the Atlantic Ocean, in The Earth's Crust and Upper Mantle, AGU Monog. 13, edited by P. J. Hart, 341-351, 1969.

Tozer, D. C. , Towards a theory of thermal convection in the earth's mantle, in The Earth's Mantle, edited by T. F. Gaskell, Academic Press, New York, 325-353, 1967.

Turcotte, D. L. , and Oxburgh, E. R. , Finite amplitude convection cells and continental drift, J. Fluid Mech. , 28, 29-42, 1967.

Turcotte, D. L. , and Oxburgh, E. R. , Convection in a mantle with variable physical properties, J. Geophys. Res. , 74, 1458-1474, 1969.

Uotila, U. A. , Gravity anomalies for a model earth, Ohio State Univ. Dept. Geodetic Sci. Tech. Rep. , 37, 15 pp. , 1962.

Veis, G. , Relation with DSIF stations, Smithsonian Astrophys. Obs. Spec. Rep. No. 200, vol. 3, 115-125, 1966.

Veis, G., Results from geometric methods, in Space Research VII, edited by R. L. Smith-Rose, S. A. Bowhill, and J. W. King, North-Holland Publ. Co., Amsterdam, 778-782, 1967a.

Veis, G., Geodetic interpretation of the results, in Space Research VII, edited by R. L. Smith-Rose, S. A. Bowhill, and J. W. King, North-Holland Publ. Co., Amsterdam, 776-777, 1967b.

Weertman, J., The creep strength of the earth's mantle, Rev. Geophys. Space Phys., 8, 145-168, 1970.

Whipple, F. L., On the satellite geodesy program at the Smithsonian Astrophysical Observatory, in Space Research VII, edited by R. L. Smith-Rose, S. A. Bowhill, and J. W. King, North-Holland Publ. Co., Amsterdam, 675-683, 1967.

Whipple, F. L., and Hynek, J. A., Optical and visual tracking of artificial satellites, in Proceedings VIIIth International Astronautical Congress, Springer-Verlag, Vienna, 429-435, 1958.